

# An energy-preserving Discrete Element Method for elastodynamics

Laurent Monasse<sup>\*,a,b</sup>, Christian Mariotti<sup>b</sup>

<sup>a</sup> *Université Paris-Est, CERMICS, 6 et 8 avenue Blaise Pascal, Cité Descartes – Champs-sur-Marne, 77455 Marne-la-Vallée Cedex 2, France*

<sup>b</sup> *CEA DIF, F-91297 Arpaçon, France*

---

## Abstract

We develop a Discrete Element Method (DEM) for elastodynamics using polyhedral elements. We show that for a given choice of forces and torques, we recover the equations of linear elastodynamics in small deformations. Furthermore, the torques and forces derive from a potential energy, and thus the global equation is an Hamiltonian dynamics. The use of an explicit symplectic time integration scheme allows us to recover conservation of energy, and thus stability over long time simulations. These theoretical results are illustrated by numerical simulations of test cases involving large displacements.

*Key words:* Discrete Element Method, Energy conservation

---

## 1. Introduction

Particle methods are meshless simulation techniques in which a continuum medium is approximated through the dynamics of a set of interacting particles. Among these, Discrete Element methods (DEM) have first been developed by Hoover, Arhurst and Olness [20] in models for crystalline materials. Their application to geotechnical problems was carried out by Cundall and Strack [4], and their use in granular materials and rock simulation is still widespread [36, 35]. The handling of a set of particles interacting by means of forces and torques enables to represent the microscale effects of the material and to model a variety of behaviour laws. The model is also able to account for size effects [21], and to treat fracture in a natural way. Granular material simulations generally use spherical elements interacting via noncohesive, frictional contact forces [36]. For brittle materials, models also use unilateral contact forces, combined with bonds which simulate cohesion [35]. Kun and Herrmann developed a combination of the contact model with a lattice model of beams to account for the cohesion [26], which has been extended to Reissner models of beams to simulate large rotations of the material [5, 21]. The authors use Voronoi tessellations to generate the polygonal particles. However, the results obtained still depend on the size of the discretization (which physically corresponds to the size of heterogeneities) [21]. The effective macroscopic Young modulus and Poisson ratio highly depend on the isotropy of the distribution of the particles and are only empirically linked to their microscopic value for the Reissner beams [26]. Discrete Element Methods have also been used to simulate thermal conduction in granular assemblies [10] or fluid-structure interaction [16].

Other particle methods are in use in continuum mechanics. Smooth Particles Hydrodynamics (SPH) was first introduced by Gingold and Monaghan [12] and Lucy [32] for compressible fluids in astrophysical applications. The method was then extended to incompressible fluids by Monaghan [34] and to elastic and plastic dynamics by Libersky *et al* [31], and used for fluid-structure interaction with both domains discretized with SPH [2]. A state of the art review of the method is presented in [19]. SPH consists in affecting a distribution of density to each particle, in the form of a kernel function. This distribution is an approximation of the partition of unity. The continuous equations of evolution of the fluid or solid material therefore induce the dynamics of the particles. SPH preserves the total mass of the system exactly. However,

---

\*Corresponding author

*Email addresses:* monassel@cermics.enpc.fr (Laurent Monasse), christian.mariotti@cea.fr (Christian Mariotti)

in tensile regime, unphysical clusters of particles tend to appear in situations where a homogeneous response is expected [39]. Hicks, Swegle and Attaway advocate the smoothing of the variables between neighbouring particles to stabilize the method, rather than introducing artificial viscosities [18]. Bonet and Lok have addressed the issue of angular momentum preservation, and show that rotational invariance is equivalent to the exact evaluation of the gradients of linear velocity fields, which can be achieved either through correction of the kernel function or through a modification of its gradient [3]. In order to circumvent these difficulties affecting SPH, Yserentant developed the Finite Mass method, in which particles of fixed size and shape also possess a rotational degree of freedom (spin). The method achieves effective partition of unity, and thus preserves momentum, angular momentum and energy, ensuring stability [40].

Another particle method is the Moving Particle Semi-implicit (MPS) method, developed by Koshizuka. It consists in the derivation of the dynamics of a set of points from a discrete Hamiltonian [23]. As in the SPH method, the differential operators are approximated by a kernel function of compact support. The expression of the approximated differential operators is inserted in the classical Hamiltonian of the system, and by application of Hamilton's equations, the dynamics of the discretized system is obtained. To preserve the Hamiltonian structure of the dynamic of the system through time discretization, the authors use symplectic schemes [38]. The MPS method has been used initially for free-surface flows [23, 24], and has been extended to nonlinear elastodynamics [25, 38] and to fluid-structure interaction [29]. Using similar ideas, by deriving the dynamics of the system from a discrete Hamiltonian, Fahrenthold has simulated compressible flows [22] and impact events with breaking of the target [8, 9].

These methods show the importance of the preservation of momentum and energy for the accuracy and stability of the scheme over long-time simulation. The use of symplectic schemes ensures the preservation of the structure of Hamilton's equations by the numerical time integration, and therefore the preservation of momentum and energy [15]. Simo, Tarnow and Wong note, however, that while ensuring the stability of the simulation for small time steps, the symplectic schemes fail to preserve exactly energy and become unstable for larger time steps [37]. They derive a general class of implicit time-stepping algorithms which exactly enforce the conservation of momentum, angular momentum and energy. The algorithms are built in order to preserve linear and angular momentum, and energy conservation is enforced either with a projection method (projection on the manifold of constant energy) or with a collocation method. The algorithm is used for nonlinear elasticity in large deformation using finite element methods [37, 13, 28] and for low-velocity impact [17].

In this article, we study a method proposed by Mariotti [33], which combines a Discrete Element Method with a lattice model. This method, CeaMka3D<sup>TM</sup>, has been successfully used to simulate e.g. the propagation of seismic waves in linear elastic medium [33]. Here, we study some properties of the algorithm in the case of a linear elastic behavior, in large displacements, and without fracture. We will first describe the discrete set of equations, and then study the properties of conservation of energy by the time-scheme. In section 2, we describe the lattice model used, and the expression of forces and torques chosen to simulate linear elasticity. In section 3, we show that these expressions lead to a macroscopic behaviour of the material equivalent to a Cosserat continuum, with a characteristic length of the order of the size of the particles. Hence, the model is consistent with a Cauchy continuum medium up to second-order accuracy, in the case of small displacement and small deformation. The microscopic values of Young modulus and Poisson ratio yield directly the macroscopic values, and we can choose Poisson ratio in the whole interval  $(-1, 0.5)$ . We also compute the dispersion relation of the scheme. In section 4, we show that the forces and torques between particles derive from an Hamiltonian function. In section 5, we then describe the symplectic RATTLE time-scheme [15], which allows us to preserve a discrete energy over long-time simulations. These theoretical results are illustrated by numerical simulations of test cases involving large displacements.

## 2. Description of the method

### 2.1. Geometrical description of the system

In order to discretize the continuum material, several methods have been suggested for Discrete Element methods. Most authors working on granular materials use hard spheres, in order to simplify the computation

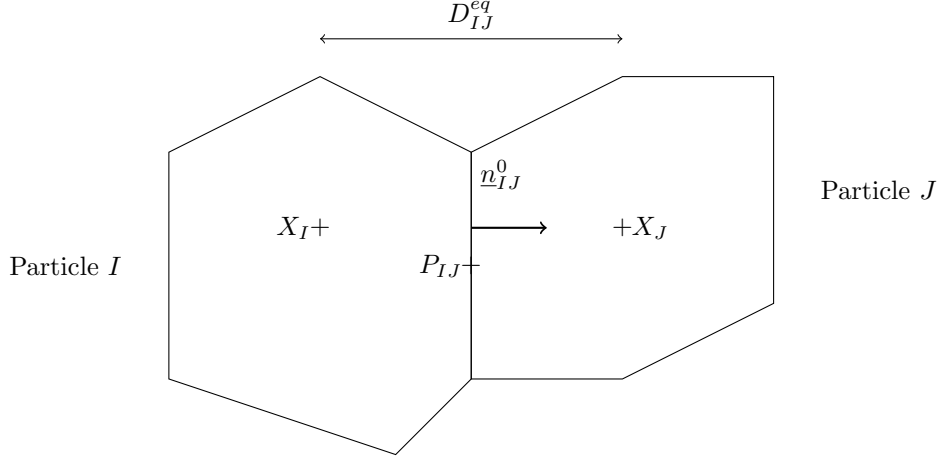


Figure 1: Geometric description of the particles

of contacts between particles, as the exact form of the particles is mainly unknown. However, in the case of the simulation of a continuous material, this method is not adapted as the interstitial vacuum between spheres is inconsistent with the compacity of the solid. In addition, the difficulty to obtain a dense packing of hard spheres, and the problem of the expression of cohesion between the particles, have led us to use Voronoi tessellations instead, as suggested in [26, 5]. The particles are therefore convex polyhedra which define a partition of the entire domain. As we shall see, this method allows us to handle any Poisson ratio  $\nu$  strictly between  $-1$  and  $0.5$ , independently from the size of the particles. On the contrary, most granular sphere packing methodologies account for a limited range of  $\nu$ , which is size dependent.

After building the Voronoi tessellation, the position of particle  $I$  is identified by the initial position of its center denoted  $X_I^0$ . The center is not necessarily the center of mass of the particle. However, when the points serving to build the Voronoi tessellation are evenly distributed, the distance between point  $X_I^0$  and the center of mass of particle  $I$  is small compared to the radius of the particle, and to simplify things, we will make the assumption that  $X_I^0$  is the center of mass of particle  $I$ . It follows from the Voronoi construction that the interface between particles  $I$  and  $J$  is orthogonal to vector  $\underline{X_I^0 X_J^0}$  and at an equal distance from  $I$  and  $J$ .

We define the following geometric parameters when starting the computation for particle  $I$  :

- its mass  $m_I$  and its volume  $V_I$ .
- its “free volume”  $V_I^l$  : when particle  $I$  has one or more interfaces with no *vis-à-vis*, these surfaces are marked as stress-free. To account for the free deformation of the particle in these directions,  $V_I^l$  is defined as the sum of the volumes of all pyramidal polyhedra with a free surface as basis and  $X_I^0$  as summit.
- the orthonormal basis  $(e_1^I, e_2^I, e_3^I)$  of the principal axes of inertia of the particle. We call it the inertial frame.
- the principal moments of inertia  $I_1, I_2$  and  $I_3$  of the particle. The matrix of inertia  $\underline{\underline{R}}_I^0$  can be written in the inertial frame :

$$\underline{\underline{R}}_I^0 = \begin{pmatrix} I_1 & 0 & 0 \\ 0 & I_2 & 0 \\ 0 & 0 & I_3 \end{pmatrix}$$

The matrix of inertia is assumed to be time-independent.

- We also need the following parameters : let

$$d_i = \frac{I_1 + I_2 + I_3}{2} - I_i, \quad i = 1, 2, 3$$

and introduce the matrix  $\underline{\underline{D}}_I$  defined in the inertial frame as :

$$\underline{\underline{D}}_I = \begin{pmatrix} d_1 & 0 & 0 \\ 0 & d_2 & 0 \\ 0 & 0 & d_3 \end{pmatrix}$$

The matrix  $\underline{\underline{D}}_I$  will be useful when describing the dynamics of the particle's rotation.

- the list  $\mathcal{V}_I$  of the neighbours of the particle.

We also define fixed parameters for each interface between particles  $I$  and  $J$  :

- $P_{IJ}$  the center of mass of the interface.  $P_{IJ}$  is not necessarily aligned with  $X_I$  and  $X_J$ .
- the surface  $S_{IJ}$  of the interface.
- the initial (equilibrium) distance between particles  $I$  and  $J$  :

$$D_{IJ}^{eq} = \|\underline{X}_I^0 \underline{X}_J^0\|$$

- the ponderation coefficient for the distance between  $X_I^0$  and the interface :  $\alpha_{IJ}^I$  is the ratio of the distance from  $X_I$  to the interface of particles  $I$  and  $J$  over distance  $D_{IJ}^{eq}$  between  $X_I^0$  and  $X_J^0$  (in general, for a Voronoi tessellation,  $\alpha_{IJ}^I = \frac{1}{2}$  . For the sake of generality, we keep the notation  $\alpha_{IJ}^I$ ).
- the initial exterior normal vector for link  $IJ$  :

$$\underline{n}_{IJ}^0 = \frac{1}{D_{IJ}^{eq}} \underline{X}_I^0 \underline{X}_J^0$$

- Two normalized principal vectors of the interface  $\underline{s}_{IJ}^0$  and  $\underline{t}_{IJ}^0$ . These orthonormal vectors are contained in the interface between particles  $I$  and  $J$ , and serve as references to evaluate the torsion between particles  $I$  and  $J$ . To fix ideas about their orientation, as  $\underline{n}_{IJ}^0$  is normal to the interface plane, we impose :

$$\underline{n}_{IJ}^0 \wedge \underline{s}_{IJ}^0 = \underline{t}_{IJ}^0$$

These parameters are determined once and for all at the initiation of the computation. The particles are therefore assumed to be rigid. However, compressibility effects are taken into account through the expression of forces.

We then determine the kinematic variables of the particle. The movement of the particle  $I$  is totally described at each time  $t$  by the position of its center of mass denoted  $\underline{X}_I$  and by its rotation matrix  $\underline{Q}_I$ . This matrix describes the rotation which carries the initial inertial frame of particle  $I$  to the inertial frame of particle  $I$  at time  $t$  in the fixed Galilean referential where the movement of the particles is computed. The matrix of inertia in the fixed frame  $\underline{R}_I$  at time  $t$  can therefore be expressed as :

$$\underline{R}_I = \underline{Q}_I \cdot \underline{R}_I^0 \cdot \underline{Q}_I^{-1} \quad (1)$$

From these kinematic variables, we derive other variables which will be useful to compute forces and torques between particles :

- The linear velocity  $\underline{v}_I$  :

$$\underline{v}_I = \frac{d\underline{X}_I}{dt}$$

- We introduce the map  $\underline{j} : \mathbb{R}^3 \rightarrow \mathbb{R}^{3 \times 3}$  such that :  $\forall \underline{x} = (x_1, x_2, x_3) \in \mathbb{R}^3$ ,

$$\underline{j}(\underline{x}) = \begin{pmatrix} 0 & -x_3 & x_2 \\ x_3 & 0 & -x_1 \\ -x_2 & x_1 & 0 \end{pmatrix}$$

As a consequence :

$$\forall \underline{x} \in \mathbb{R}^3, \forall \underline{y} \in \mathbb{R}^3, \underline{j}(\underline{x}) \cdot \underline{y} = \underline{x} \wedge \underline{y}$$

- The rotation velocity vector in the fixed frame : this vector  $\underline{\Omega}_I \in \mathbb{R}^3$  is such that :

$$\underline{j}(\underline{\Omega}_I) = \frac{d\underline{Q}}{dt} \underline{Q}^T \quad (2)$$

Since  $\underline{Q}$  is an orthogonal matrix,  $\frac{d\underline{Q}}{dt} \underline{Q}^T$  is skew-symmetric and  $\underline{\Omega}_I$  indeed exists.

- The rotation velocity vector in the inertial frame : this vector  $\underline{\omega}_I \in \mathbb{R}^3$  is such that :

$$\underline{j}(\underline{\omega}_I) = \underline{Q}^T \frac{d\underline{Q}}{dt}$$

The following relation links these two rotation velocity vectors :

$$\underline{\Omega}_I = \underline{Q} \cdot \underline{\omega}_I \quad (3)$$

- The distance between particles  $I$  and  $J$  at time  $t$  :

$$D_{IJ} = \|\underline{X}_J - \underline{X}_I\|$$

- The exterior normal vector for link  $IJ$  at time  $t$  :

$$\underline{n}_{IJ} = \frac{1}{D_{IJ}} (\underline{X}_J - \underline{X}_I)$$

- The difference between points  $P_{IJ}^I$  and  $P_{IJ}^J$  : point  $P_{IJ}^I$  is defined as the position of point  $P_{IJ}$  at time  $t$  under the rigid body movement of particle  $I$ , and conversely, point  $P_{IJ}^J$  is defined as the position of point  $P_{IJ}$  at time  $t$  under the rigid body movement of particle  $J$ . By definition,

$$\underline{X}_I P_{IJ}^I = \underline{Q}_I \underline{X}_I^0 P_{IJ} \quad \text{and} \quad \underline{X}_J P_{IJ}^J = \underline{Q}_J \underline{X}_J^0 P_{IJ}$$

The difference can therefore be described as the following vector :

$$\begin{aligned} \underline{\Delta u}_{IJ} &= P_{IJ}^I P_{IJ}^J \\ &= \underline{X}_J - \underline{X}_I + \underline{Q}_J \cdot \underline{X}_J^0 P_{IJ} - \underline{Q}_I \cdot \underline{X}_I^0 P_{IJ} \end{aligned}$$

- The volumic deformation  $\varepsilon_I^v$  of particle  $I$  : it is defined as the sum of all contributions of the deformations of the links between particle  $I$  and the surrounding particles. We have assumed that the bending of the link between two particles does not affect volume, as long as the centers of the interface of the two particles stay in contact.

$$\varepsilon_I^v = \sum_{J \in \mathcal{V}_I} \frac{\alpha_{IJ}^I S_{IJ}}{V_I + 3 \frac{\nu}{1-2\nu} V_I^I} \underline{\Delta u}_{IJ} \cdot \underline{n}_{IJ}$$

- The interpolated volumic deformation for link  $(IJ)$  :

$$\varepsilon_{IJ}^v = \alpha_{IJ}^I \varepsilon_I^v + \alpha_{IJ}^J \varepsilon_J^v$$

## 2.2. Expression of the forces and torques

We can now give the expression of forces and torques between particles. The following expression of forces has been fitted to simulate the behavior of a linear elastic material, but other expressions for the forces, modeling nonlinear laws for the material, are able to yield more complex and realistic behaviors. It is also possible to add damping forces to dissipate energy in the material.

We denote by  $E$  the Young's modulus and by  $\nu$  the Poisson's ratio for the material. We have the following expression for the normal force by particle  $J$  onto particle  $I$  :

$$\underline{F}_{IJ}^n = S_{IJ} \frac{E}{1+\nu} \frac{D_{IJ} - D_{IJ}^{eq}}{D_{IJ}^{eq}} \underline{n}_{IJ} + S_{IJ} \frac{E\nu}{(1+\nu)(1-2\nu)} \varepsilon_{IJ}^v \underline{n}_{IJ}^\perp \quad (4)$$

with

$$\underline{n}_{IJ}^\perp = \underline{n}_{IJ} + \frac{1}{D_{IJ}} (\underline{\Delta} u_{IJ} - (\underline{\Delta} u_{IJ} \cdot \underline{n}_{IJ}) \underline{n}_{IJ})$$

This force represents the compression force between particles. Although, at first sight, the second part of  $\underline{n}_{IJ}^\perp$  could be neglected in small displacements, its presence is necessary to derive the force from a potential energy.

For the tangential force applied by particle  $J$  onto particle  $I$ , we choose the following expression :

$$\underline{F}_{IJ}^t = \frac{S_{IJ}}{D_{IJ}^{eq}} \frac{E}{1+\nu} \left( D_{IJ}^{eq} \underline{n}_{IJ} + \underline{Q}_J \cdot \underline{X}_J^0 P_{IJ} - \underline{Q}_I \cdot \underline{X}_I^0 P_{IJ} \right) \quad (5)$$

This force is the shear force between particles.

If we sum those two forces, we get the total force applied by particle  $J$  onto particle  $I$ , whose expression is much simpler and will be used in section 4 for the conservation of energy :

$$\underline{F}_{IJ} = \frac{S_{IJ}}{D_{IJ}^{eq}} \frac{E}{1+\nu} \underline{\Delta} u_{IJ} + S_{IJ} \frac{E\nu}{(1+\nu)(1-2\nu)} \varepsilon_{IJ}^v \underline{n}_{IJ}^\perp \quad (6)$$

This expression can be compared with Hooke's law of linear elasticity :

$$\underline{\underline{\sigma}} = \frac{E}{1+\nu} \underline{\underline{\varepsilon}} + \frac{E\nu}{(1+\nu)(1-2\nu)} \text{tr}(\underline{\underline{\varepsilon}}) \underline{\underline{I}} \quad (7)$$

where  $\underline{\underline{\sigma}}$  denotes the stress tensor and  $\underline{\underline{\varepsilon}}$  the strain tensor. The first term of equation (7) corresponds to the first term of equation (6) (it is the contribution of the deformation of link  $(IJ)$  alone), and the second term of equation (7) corresponds to the second term of equation (6) (it is the contribution of the global deformation of particle  $I$  to the normal force).

The first torque to be considered is the torque induced by the total force at the center of mass of the particle :

$$\underline{M}_{IJ}^t = \underline{P}_{IJ}^I \underline{X}_I \wedge \underline{F}_{IJ} = -\frac{S_{IJ}}{D_{IJ}^{eq}} \frac{E}{1+\nu} (\underline{Q}_J \cdot \underline{X}_J^0 P_{IJ}) \wedge \underline{\Delta} u_{IJ} + \frac{E\nu}{(1+\nu)(1-2\nu)} \varepsilon_{IJ}^v S_{IJ} \underline{X}_I P_{IJ}^I \wedge \underline{n}_{IJ} \quad (8)$$

In addition, we need to consider the torques representing the bending and the torsion of the link between particles  $I$  and  $J$ . We need to recover the behavior of the material under torsion and bending, that is, if we denote  $R_{IJ}^s$  and  $R_{IJ}^t$  the principal moments of inertia of the surface between particles  $I$  and  $J$  associated with the principal axes  $\underline{s}_{IJ}^0$  and  $\underline{t}_{IJ}^0$ , we should have the bending moment of the form :

$$\underline{M}_{IJ}^f = \frac{E}{D_{IJ}^{eq}} (R_{IJ}^s \phi_s \underline{s}_{IJ}^0 + R_{IJ}^t \phi_t \underline{t}_{IJ}^0) + \frac{E}{D_{IJ}^{eq}(1+\nu)} (R_{IJ}^s + R_{IJ}^t) \phi_n \underline{n}_{IJ} \quad (9)$$

where we have supposed that bending and torsion are small, and where we denote  $\phi_n$ ,  $\phi_s$  and  $\phi_t$  the respective torsion angle around axis  $\underline{n}_{IJ}$ , and the bending angles around axes  $\underline{s}_{IJ}^0$  and  $\underline{t}_{IJ}^0$ .

To compute angles  $\phi_n$ ,  $\phi_s$  and  $\phi_t$ , we use the relative rotation of the axes  $\underline{n}_{IJ}^0$ ,  $\underline{s}_{IJ}^0$  and  $\underline{t}_{IJ}^0$  under the rigid body movements of particles  $I$  and  $J$ . However, as the three movements are combined in large rotations of the particles, we rather set :

$$\underline{M}_{IJ}^f = \frac{E S_{IJ}}{D_{IJ}^{eq}} \left( \alpha_n (\underline{Q} \cdot \underline{n}_{IJ}^0) \wedge (\underline{Q} \cdot \underline{n}_{IJ}^0) + \alpha_s (\underline{Q} \cdot \underline{s}_{IJ}^0) \wedge (\underline{Q} \cdot \underline{s}_{IJ}^0) + \alpha_t (\underline{Q} \cdot \underline{t}_{IJ}^0) \wedge (\underline{Q} \cdot \underline{t}_{IJ}^0) \right) \quad (10)$$

where coefficients  $\alpha_n$ ,  $\alpha_s$  and  $\alpha_t$  have to be determined to yield equation (9) in the case of small rotations. We therefore have :

$$\alpha_n = \frac{\nu(R_{IJ}^s + R_{IJ}^t)}{2(1 + \nu)S_{IJ}} \quad (11)$$

$$\alpha_s = \frac{(2 + \nu)R_{IJ}^t - \nu R_{IJ}^s}{2(1 + \nu)S_{IJ}} \quad (12)$$

$$\alpha_t = \frac{(2 + \nu)R_{IJ}^s - \nu R_{IJ}^t}{2(1 + \nu)S_{IJ}} \quad (13)$$

For simplicity, we will continue to note these coefficients  $\alpha_n$ ,  $\alpha_s$  and  $\alpha_t$  and we will use their explicit expression only when needed.

We define the total torque applied by particle  $J$  onto particle  $I$  :

$$\underline{M}_{IJ} = \underline{M}_{IJ}^t + \underline{M}_{IJ}^f$$

With these forces and torques, the model is now complete. The dynamics of the system is then defined as Newton's dynamics for each particle subject to the sum of forces and torques :

$$m_I \ddot{\underline{X}}_I = \sum_{J \in \mathcal{V}_I} \underline{F}_{IJ} + \underline{F}_I^{ext} \quad (14)$$

$$\frac{d}{dt} (\underline{R}_I \cdot \underline{\Omega}_I) = \sum_{J \in \mathcal{V}_I} \underline{M}_{IJ} + \underline{M}_I^{ext} \quad (15)$$

### 3. Consistency and accuracy of the scheme

In this section, we establish the consistency and the accuracy of the scheme. We first present the equivalent equation for displacement and rotation in small displacements and small deformations. As the equations obtained are coupled dynamics for displacement and rotation, we compare the model with Cosserat generalized continuum, and recover a Cauchy continuum. The spectral analysis of the scheme exhibits a superposition of low frequency waves and high frequency waves. The low frequency waves propagate at celerities consistent with elastodynamics and satisfy relation  $\underline{\theta} = \frac{1}{2} \underline{\text{rot}}(\underline{\xi})$ . The high frequency waves exhibit frequencies which depend on the size of the spatial discretization : they are the propagation of the initial error and are determined solely by the initial conditions. Finally, we compare our results with numerical tests.

#### 3.1. Equivalent equation for the scheme

We need to simplify the geometrical configuration to be able to develop an equivalent equation for the scheme. We therefore place the points of the Voronoi tessellation on a Cartesian grid, which reduces the general discrete element formulation to a "finite difference" scheme. The different parameters are therefore simplified :

- We set  $\Delta x$ ,  $\Delta y$  and  $\Delta z$  the initial distance between particles along axes  $x$ ,  $y$  and  $z$  respectively.

- The particles are therefore rectangular parallelepipeds whose center of mass is initially located at  $\underline{X}_I^0 = (j\Delta x, k\Delta y, l\Delta z)$  where  $j$ ,  $k$  and  $l$  are integers.
- The center of mass  $P_{IJ}$  of the interface between particles  $I$  and  $J$  is aligned with  $X_I$  and  $X_J$ , and therefore :

$$\underline{X}_I^0 P_{IJ} = \frac{D_{IJ}^{eq}}{2} \underline{n}_{IJ}^0$$

- The mass  $m_I$  is defined by :  $m_I = \rho_I \Delta x \Delta y \Delta z$  where  $\rho_I$  denotes the density of particle  $I$ .
- The inertia matrix  $\underline{R}_I$  has the following expression in the frame  $(\underline{e}_x, \underline{e}_y, \underline{e}_z)$  :

$$\underline{R}_I = \Delta x \Delta y \Delta z \rho_I \begin{pmatrix} M_x & 0 & 0 \\ 0 & M_y & 0 \\ 0 & 0 & M_z \end{pmatrix}$$

with

$$M_x = \frac{\Delta y^2 + \Delta z^2}{12}$$

$$M_y = \frac{\Delta x^2 + \Delta z^2}{12}$$

$$M_z = \frac{\Delta x^2 + \Delta y^2}{12}$$

- Surface  $S_{IJ}$  :

$$S_{IJ} = \frac{\Delta x \Delta y \Delta z}{D_{IJ}^{eq}}$$

- The principal moments of inertia of the surface between particles  $I$  and  $J$  on principal vectors  $\underline{s}_{IJ}^0$  and  $\underline{t}_{IJ}^0$ , which we denoted  $R_{IJ}^s$  and  $R_{IJ}^t$  : if we suppose for example that  $\underline{n}_{IJ}^0 = \underline{e}_x$ , we then have  $\underline{s}_{IJ}^0 = \underline{e}_y$  and  $\underline{t}_{IJ}^0 = \underline{e}_z$ , and we get :

$$R_{IJ}^s = \frac{\Delta y \Delta z^3}{12}, \quad R_{IJ}^t = \frac{\Delta y^3 \Delta z}{12}$$

and we have the same result for the other configurations with permutation of indices  $x$ ,  $y$  and  $z$ .

- $\alpha_{IJ}^I$  is always equal to  $\frac{1}{2}$ .
- The orthonormal basis  $(\underline{n}_{IJ}^0, \underline{s}_{IJ}^0, \underline{t}_{IJ}^0)$  is a permutation of the standard orthonormal basis  $(\underline{e}_x, \underline{e}_y, \underline{e}_z)$ ,  $\underline{n}_{IJ}^0$  being aligned with  $X_I$  and  $X_J$  and pointing from  $I$  to  $J$ .

We assume to have no exterior force applied on the system. We consider the displacement of particle  $I$  :

$$\underline{\xi}_I = \underline{X}_I - \underline{X}_I^0$$

We assume that  $\underline{\xi}$  is a regular function on the domain, and we can therefore expand  $\underline{\xi}_J$  at point  $I$  with Taylor series if  $J \in \mathcal{V}_I$ . We denote  $h$  the greatest of  $\Delta x$ ,  $\Delta y$  and  $\Delta z$ .

In addition, we assume that displacements and rotations are small for particles. We note that rotations can be written :

$$\underline{Q}_I = \begin{pmatrix} 1 & -\theta_z^I & \theta_y^I \\ \theta_z^I & 1 & -\theta_x^I \\ -\theta_y^I & \theta_x^I & 1 \end{pmatrix} + \mathcal{O}(\theta_x^2, \theta_y^2, \theta_z^2)$$

where  $\theta_x^I$ ,  $\theta_y^I$  and  $\theta_z^I$  denote the respective small rotation angles around axes  $x$ ,  $y$  and  $z$ . We also expand  $\underline{\theta}_J$  with Taylor series at point  $I$ .



Using (14), (6) and the symmetry of the problem to simplify a number of terms of the Taylor series, we eventually get for the displacement :

$$\begin{aligned} \rho \ddot{\xi}_x = & \frac{E}{1+\nu} \left( \frac{\partial^2 \xi_x}{\partial x^2} + \frac{\partial^2 \xi_x}{\partial y^2} + \frac{\partial^2 \xi_x}{\partial z^2} + \frac{\partial \theta_z}{\partial y} - \frac{\partial \theta_y}{\partial z} \right) + \frac{E\nu}{(1+\nu)(1-2\nu)} \left( \frac{\partial^2 \xi_x}{\partial x^2} + \frac{\partial^2 \xi_y}{\partial x \partial y} + \frac{\partial^2 \xi_z}{\partial x \partial z} \right) \\ & + \frac{E}{1+\nu} \left( \frac{\Delta x^2}{12} \frac{\partial^4 \xi_x}{\partial x^4} + \frac{\Delta y^2}{12} \frac{\partial^4 \xi_x}{\partial y^4} + \frac{\Delta z^2}{12} \frac{\partial^4 \xi_x}{\partial z^4} + \frac{\Delta y^2}{6} \frac{\partial^3 \theta_z}{\partial y^3} - \frac{\Delta z^2}{6} \frac{\partial^3 \theta_y}{\partial z^3} \right) \\ & + \frac{E\nu}{(1+\nu)(1-2\nu)} \left( \frac{\Delta x^2}{3} \frac{\partial^4 \xi_x}{\partial x^4} + \frac{\Delta x^2}{6} \frac{\partial^4 \xi_y}{\partial x^3 \partial y} + \frac{\Delta x^2}{6} \frac{\partial^4 \xi_z}{\partial x^3 \partial z} + \frac{\Delta y^2}{6} \frac{\partial^4 \xi_y}{\partial x \partial y^3} + \frac{\Delta z^2}{6} \frac{\partial^4 \xi_z}{\partial x \partial z^3} \right) \\ & + \mathcal{O}(h^3) \quad (16) \end{aligned}$$

The same results hold for  $\xi_y$  and  $\xi_z$  permuting the indices  $x$ ,  $y$  and  $z$  circularly.

In the same way, using (15), (8) and (10), and using the expressions (11),(12) and (13) of  $\alpha_n$ ,  $\alpha_s$  and  $\alpha_t$ , we get for the rotation :

$$\begin{aligned} \frac{\Delta y^2 + \Delta z^2}{12} \rho \ddot{\theta}_x = & \frac{E}{1+\nu} \left( \frac{\partial \xi_z}{\partial y} - \frac{\partial \xi_y}{\partial z} - 2\theta_x + \frac{\Delta y^2}{6} \frac{\partial^3 \xi_z}{\partial y^3} - \frac{\Delta z^2}{6} \frac{\partial^3 \xi_y}{\partial z^3} + \frac{\Delta y^4}{120} \frac{\partial^5 \xi_z}{\partial y^5} \right. \\ & \left. - \frac{\Delta z^4}{120} \frac{\partial^5 \xi_y}{\partial z^5} - \frac{\Delta y^2}{4} \frac{\partial^2 \theta_x}{\partial y^2} - \frac{\Delta z^2}{4} \frac{\partial^2 \theta_x}{\partial z^2} - \frac{\Delta y^4}{48} \frac{\partial^4 \theta_x}{\partial y^4} - \frac{\Delta z^4}{48} \frac{\partial^4 \theta_x}{\partial z^4} \right) \\ & + E \left[ \frac{\Delta y^2 + \Delta z^2}{12(1+\nu)} \left( \frac{\partial^2 \theta_x}{\partial x^2} + \frac{\Delta x^2}{12} \frac{\partial^4 \theta_x}{\partial x^4} \right) + \frac{\Delta z^2}{12} \left( \frac{\partial^2 \theta_x}{\partial y^2} + \frac{\Delta y^2}{12} \frac{\partial^4 \theta_x}{\partial y^4} \right) \right. \\ & \left. + \frac{\Delta y^2}{12} \left( \frac{\partial^2 \theta_x}{\partial z^2} + \frac{\Delta z^2}{12} \frac{\partial^4 \theta_x}{\partial z^4} \right) \right] + \mathcal{O}(h^5) \quad (17) \end{aligned}$$

The same results hold for  $\theta_y$  and  $\theta_z$  permuting the indices  $x$ ,  $y$  and  $z$  circularly.

We see that these sets of equations couple  $\underline{\xi}$  and  $\underline{\theta}$ , and by construction of the method, no constitutive law exists between  $\underline{\xi}$  and  $\underline{\theta}$ . However, we are looking for the equivalent equation for the spatial scheme, that is, the equation which is best approximated by the scheme. The fact that a rotation remains in the equations can be compared to Cosserat continuum theory. We investigate this comparison in the following subsection, and show how we recover classical Cauchy continuum theory as the spatial discretization step tends to 0.

### 3.2. Comparison with Cosserat and Cauchy continuum theories

In a Cosserat model for continuum media, the kinematics is described by a displacement field  $\underline{u}$  and a rotation field  $\underline{\phi}$ . A modified strain tensor  $\underline{\underline{\varepsilon}}$  and a new curvature strain tensor  $\underline{\underline{\kappa}}$  are introduced [7] :

$$\begin{aligned} \underline{\underline{\varepsilon}} &= \underline{\underline{\text{grad}}} \underline{u} + \underline{j}(\underline{\phi}) \\ \underline{\underline{\kappa}} &= \underline{\underline{\text{grad}}} \underline{\phi} \end{aligned}$$

We define  $\underline{\underline{t}}$  and  $\underline{\underline{\mu}}$  the stress and couple stress tensors. We assume the following constitutive relations :

$$\underline{\underline{t}} = \lambda \text{tr}(\underline{\underline{\varepsilon}}) \underline{\underline{Id}} + \mu \underline{\underline{\varepsilon}} + \mu_c \underline{\underline{\varepsilon}}^T \quad (18)$$

$$\underline{\underline{\mu}} = \alpha \text{tr}(\underline{\underline{\kappa}}) \underline{\underline{Id}} + \gamma \underline{\underline{\kappa}} + \beta \underline{\underline{\kappa}}^T \quad (19)$$

where  $\lambda$ ,  $\mu$ ,  $\mu_c$ ,  $\alpha$ ,  $\beta$  and  $\gamma$  are elastic moduli.

The dynamical equations for the system are :

$$\begin{aligned} \rho \ddot{\underline{u}} &= \underline{\underline{\text{div}}} \underline{\underline{t}} \\ \underline{\underline{I}}_c \ddot{\underline{\phi}} &= \underline{\underline{\text{div}}} \underline{\underline{\mu}} + \underline{\underline{e}} : \underline{\underline{t}} \end{aligned}$$

where  $\rho$  denotes the density,  $\underline{\underline{I}}_c$  is a characteristic inertia matrix,  $:$  denotes the double contraction product of tensors, and  $\underline{\underline{e}}$  is defined as follows :

$$(\underline{\underline{e}})_{ijk} = \begin{cases} 1 & \text{if } (ijk) \text{ is an even permutation} \\ -1 & \text{if } (ijk) \text{ is an odd permutation} \\ 0 & \text{otherwise} \end{cases}$$

Using the constitutive relations (18) and (19), the following equations can be obtained :

$$\rho \ddot{\underline{u}} = (\lambda + \mu_c) \underline{\text{grad}} \text{ div } \underline{u} + \mu \Delta \underline{u} + (\mu - \mu_c) \underline{\text{rot}} \underline{\phi} \quad (20)$$

$$\underline{\underline{I}}_c \ddot{\underline{\phi}} = (\alpha + \beta) \underline{\text{grad}} \text{ div } \underline{\phi} + \gamma \Delta \underline{\phi} - 2(\mu - \mu_c) \underline{\phi} + (\mu - \mu_c) \underline{\text{rot}} \underline{u} \quad (21)$$

Identifying the terms of (20) with equation (16), we find :

$$\begin{aligned} \lambda &= \frac{E\nu}{(1+\nu)(1-2\nu)} \\ \mu &= \frac{E}{1+\nu} \\ \mu_c &= 0 \end{aligned}$$

and we therefore recover the classical expression, for Cauchy media, of the first Lamé coefficient  $\lambda_{Cauchy}$ , and  $\frac{\mu+\mu_c}{2}$  corresponds to the classical second Lamé coefficient  $\mu_{Cauchy}$ . Comparing then equation (21) with equation (17), we find :

$$\underline{\underline{I}}_c = \rho \begin{pmatrix} \frac{\Delta y^2 + \Delta z^2}{12} & 0 & 0 \\ 0 & \frac{\Delta x^2 + \Delta z^2}{12} & 0 \\ 0 & 0 & \frac{\Delta x^2 + \Delta y^2}{12} \end{pmatrix}$$

Assuming :

$$\begin{aligned} \alpha + \beta &= 0 \\ \gamma &= \frac{E}{2(1+\nu)} h^2 \end{aligned}$$

for a fixed  $h$ , we therefore see that the equivalent equations for the scheme are those of a Cosserat generalized continuum, with second-order accuracy.

One of the main characteristics of a Cosserat generalized continuum is to exhibit a characteristic length for the material,  $l_c$ , which describes the length of the nonlocal interactions.  $l_c$  is defined as :

$$l_c^2 = \frac{\gamma}{\mu + \mu_c}$$

In our case, we see that :

$$l_c = \frac{\sqrt{2}}{2} h$$

$l_c$  is of the same order as the size of the particles. In an homogenization analysis framework, S. Forest, F. Pradel and K. Sab have shown [11] that when the macroscopic length of the system is fixed and the characteristic length  $l_c$  of the Cosserat continuum tends to 0, the macroscopic behavior of the material is that of a Cauchy continuum. We therefore converge to a Cauchy continuum as  $h$  tends to 0.

As a consequence, displacement  $\underline{\xi}$ , acceleration  $\ddot{\underline{\xi}}$ , rotation  $\underline{\theta}$  and acceleration of rotation  $\ddot{\underline{\theta}}$  in equations (16) and (17) converge to finite macroscopic quantities. Therefore, using the equations on rotation, we find :

$$\underline{\theta} = \frac{1}{2} \underline{\text{rot}} \underline{\xi} + \mathcal{O}(h^2) \quad (22)$$

which is the classical definition of the local rotation of a Cauchy material at order 2. Using this relation in the equations of displacement, we find the equations of linear elasticity for a Cauchy continuum medium up to error terms of order  $\mathcal{O}(h^2)$  :

$$\rho \ddot{\underline{\xi}} = \frac{E}{2(1+\nu)} \Delta \underline{\xi} + \frac{E\nu}{(1+\nu)(1-2\nu)} \underline{\text{grad}} \text{ div } \underline{\xi} + \mathcal{O}(h^2)$$

and taking  $\frac{1}{2} \underline{\text{rot}}$  of this equation, we find the equivalent equation on rotation up to error terms of order  $\mathcal{O}(h^2)$  :

$$\rho \ddot{\underline{\theta}} = \frac{E}{2(1+\nu)} \Delta \underline{\theta} + \mathcal{O}(h^2) \quad (23)$$

We recover a second-order accuracy on the rotation  $\underline{\theta}$ . As equation (22) shows,  $\underline{\theta}$  is a derivate of  $\underline{\xi}$ , and we should expect only first-order accuracy. We have therefore improved the accuracy on  $\underline{\theta}$ .

### 3.3. Spectral analysis of the equivalent equation

We restrict ourselves to the study of the dispersion in the two-dimensional case, in the particular case when  $\Delta x = \Delta y = h$ . The three-dimensional case would be handled with the same method, but eigenvalues of a  $6 \times 6$ -matrix must be found, as we will see, which cannot be carried out explicitly.

We consider an infinite lattice of points, indexed by  $j$  and  $l$  :  $\square_{j,l}$  is the value of variable  $\square$  at the point of coordinates  $(jh, lh)$ . Linearizing the expression of forces when  $\xi_x, \xi_y$  and  $\theta$  are close to zero, we find :

$$\begin{aligned} \rho \ddot{\xi}_{j,l}^x = & \frac{E}{1+\nu} \left( \frac{\xi_{j+1,l}^x + \xi_{j-1,l}^x + \xi_{j,l+1}^x + \xi_{j,l-1}^x - 4\xi_{j,l}^x}{h^2} + \frac{\theta_{j,l+1} - \theta_{j,l-1}}{2h} \right) \\ & + \frac{E\nu}{4(1+\nu)(1-2\nu)} \left( \frac{\xi_{j+2,l}^x - 2\xi_{j,l}^x + \xi_{j-2,l}^x}{h^2} + \frac{\xi_{j+1,l+1}^y - \xi_{j+1,l-1}^y + \xi_{j-1,l-1}^y - \xi_{j-1,l+1}^y}{h^2} \right) \\ & + \mathcal{O}(\|\underline{\xi}\|^2, |\theta|^2) \end{aligned}$$

Similar results hold for  $\xi_y$  and  $\xi_z$  permuting indices  $x, y$  and  $z$  circularly.

We assume that the numerical values are the values of a plane monochromatic wave at the discretization points, with angular frequency  $\omega$  and wave vector  $\underline{k}$ . We set :

$$\begin{aligned} \xi_{j,l} &= \underline{\xi}_0 \exp i(\omega t - k_x j h - k_y l h) \\ \theta_{j,l} &= \theta_0 \exp i(\omega t - k_x j h - k_y l h) \end{aligned}$$

where  $i^2 = -1$ . Setting  $\underline{X}_0 = (\xi_0^x, \xi_0^y, \theta_0)^T$ , we have :

$$-\rho \omega^2 \underline{X}_0 = \underline{\underline{A}} \cdot \underline{X}_0$$

If we denote :

$$\begin{aligned} c_x &= \cos(k_x h), \quad c_y = \cos(k_y h) \\ s_x &= \sin(k_x h), \quad s_y = \sin(k_y h) \end{aligned}$$

$$C = 2c_x + 2c_y - 4$$

with  $\lambda = \frac{E\nu}{(1+\nu)(1-2\nu)}$  and  $\mu = \frac{E}{2(1+\nu)}$  the Lamé coefficients,  $\underline{\underline{A}}$  has the following expression :

$$\underline{\underline{A}} = \begin{pmatrix} \frac{2\mu C}{h^2} - \frac{\lambda s_x^2}{h^2} & -\frac{\lambda s_x s_y}{h^2} & -\frac{2i\mu s_y}{h} \\ -\frac{\lambda s_x s_y}{h^2} & \frac{2\mu C}{h^2} - \frac{\lambda s_y^2}{h^2} & \frac{2i\mu s_x}{h} \\ \frac{12\mu i}{h^2} \frac{s_y}{h} & -\frac{12\mu i}{h^2} \frac{s_x}{h} & -\frac{3\mu(C+8)}{h^2} + \frac{E}{2h^2} C \end{pmatrix}$$

Matrix  $\underline{A}$  has three eigenvalues. A first eigenvalue is associated with the following dispersion relation :

$$\rho\omega^2 = \frac{E}{1+\nu} \frac{4-2c_x-2c_y}{h^2} + \frac{E\nu}{(1+\nu)(1-2\nu)} \frac{s_x^2 + s_y^2}{h^2} \quad (24)$$

and eigenvector  $(s_x, s_y, 0)^T$ . This wave is the P-wave : linearizing equation (24) when  $\underline{k} = o(1/h)$ , we get the dispersion relation of the compressive wave at order 2 :

$$\rho\omega^2 = \frac{E(1-\nu)}{(1+\nu)(1-2\nu)} \|\underline{k}\|^2 - \frac{h^2}{12} \frac{E(1+2\nu)}{(1+\nu)(1-2\nu)} (k_x^4 + k_y^4) + \mathcal{O}(h^4)$$

and the eigenvector is  $(k_x, k_y, 0)^T$  at order 2.

Setting :

$$\Delta = (4+2\nu + (4-\nu)(c_x + c_y))^2 + 24(s_x^2 + s_y^2)$$

a second eigenvalue can be written for  $\underline{A}$  :

$$\rho\omega^2 = \frac{E}{1+\nu} \frac{6+\nu - \frac{\nu}{2}(c_x + c_y) - \frac{1}{2}\sqrt{\Delta}}{h^2} \quad (25)$$

associated with the eigenvector :

$$(-s_y, s_x, \frac{i}{h}(2+\nu + \frac{4-\nu}{2}(c_x + c_y) - \frac{1}{2}\sqrt{\Delta}))^T$$

Linearizing equation (25), we find the dispersion relation for the transverse S-wave at order 2 :

$$\rho\omega^2 = \frac{E}{2(1+\nu)} \|\underline{k}\|^2 + \frac{h^2}{12} \frac{E}{1+\nu} (k_x^4 + k_y^4) - \frac{(3-\nu)h^2}{48} \frac{E}{1+\nu} (k_x^2 + k_y^2)^2 + \mathcal{O}(h^4)$$

and eigenvector  $(k_y, -k_x, \frac{i(k_x^2 + k_y^2)}{2})^T$  at order 2.

The third wave is associated with the dispersion relation :

$$\rho\omega^2 = \frac{E}{1+\nu} \frac{6+\nu - \frac{\nu}{2}(c_x + c_y) + \frac{1}{2}\sqrt{\Delta}}{h^2} \quad (26)$$

and eigenvector :

$$(-s_y, s_x, \frac{i}{h}(2+\nu + \frac{4-\nu}{2}(c_x + c_y) + \frac{1}{2}\sqrt{\Delta}))^T$$

When linearized, we can see that this wave yields a local, high-frequency vibration equation as  $h$  tends to zero :

$$\rho\omega^2 = \frac{12E}{h^2(1+\nu)} - \frac{(1-\nu)E}{2(1+\nu)} \|\underline{k}\|^2 + \mathcal{O}(h^2)$$

and the form of the normalized linearized eigenvector,  $(\frac{ik_y h^2}{12}, -\frac{ik_x h^2}{12}, 1)^T$ , shows that this vibration is mainly due to spurious rotations. We can interpret this vibration wave as the propagation of the initial incompatibility between rotation and displacement : we have seen in section 3.2 that as  $h$  tends to zero, we should have  $\underline{\theta} = \frac{1}{2} \text{rot } \underline{\xi}$ . The vibration wave is the only of the three waves not to respect this relation at order 2. When the initial conditions fail to verify this condition, most of this error is therefore transferred into the vibration wave. On the contrary, as observed numerically, if the compatibility of rotation and displacement is respected initially, the local rotation vibrations remain small.

### 3.4. Numerical results

The code CeaMka3D™ is a parallel code handling three-dimensional problems. However, for practical reasons such as limitation of CPU time available, we have studied accuracy only on a two-dimensional version of the code. The same type of results would hold in three dimensions. The two-dimensional problem also has the advantage of generating a non-attenuating Rayleigh wave, which is a difficult property to recover.

We have simulated Lamb’s problem (see [27]) : a semi-infinite plane is described by a rectangular domain, with a free surface on the upper side, and absorbing conditions on the other sides (see figure 2). To prevent numerical reflection on these sides to interfere with our results, we have placed the sensors far enough from these sides. On a surface particle, we apply a vertical force, whose time evolution is described by a Ricker function (the second derivative of a Gaussian function). We should then observe the propagation of three waves : inside the domain, a compression wave of type P and a shear wave of type S, and on the surface, a Rayleigh wave. We also have a P-S wave linking the P and the S waves, which is a conversion of the P wave into an S wave after reflection at the surface. In the case of a two-dimensional problem, the intensity of P and S waves is inversely proportional to the distance to the source, and the intensity of the Rayleigh wave has to be preserved throughout its propagation.

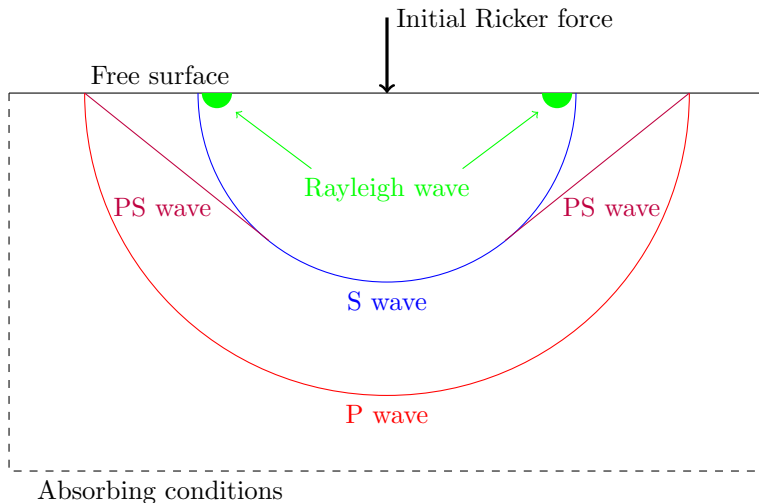


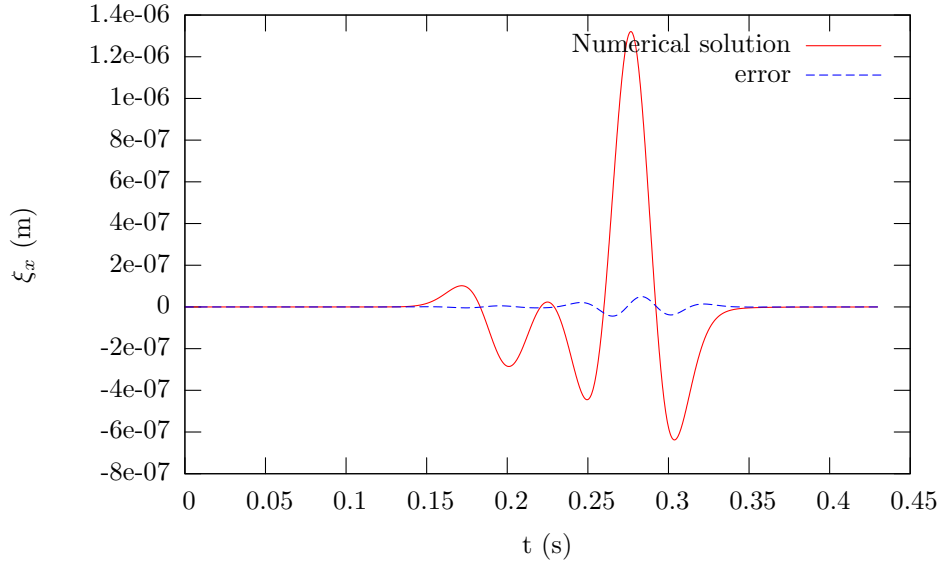
Figure 2: Schematic description of Lamb’s problem

We have chosen the following characteristics for the material : the density is  $\rho = 2200 \text{ kg.m}^{-3}$ , the Poisson coefficient is  $\nu = 0.25$ , Young’s modulus is  $E = 1.88.10^{10} \text{ Pa}$ . The velocity of P waves is therefore approximately  $3202 \text{ m.s}^{-1}$  and the velocity of S waves is  $1849 \text{ m.s}^{-1}$ .

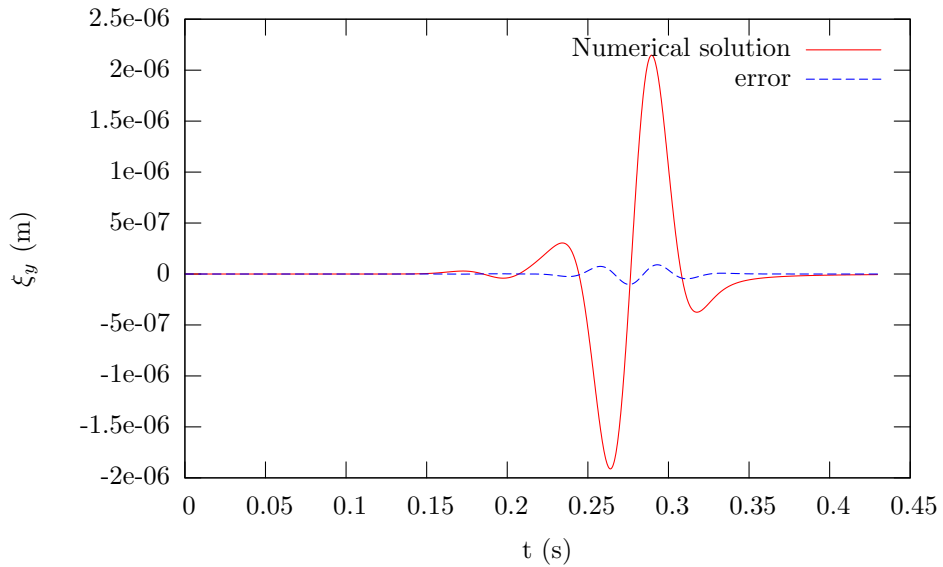
The force applied is a Ricker of central frequency 14.5 Hz, that is, with maximal frequency around 40 Hz. The minimal wave length for P waves is therefore 80 m, and the minimal wave length for S waves is approximately 50 m. In the rest of this subsection, we call “wave length” this minimal wave length of 50 m. We indicate the discretization step in terms of “number of elements per wave length”.

Lamb’s problem has the interesting particularity of having a semi-analytic solution : Cagniard’s method is described for example in [6]. We can compare the results we obtained with this exact solution and thus estimate the numerical error of the scheme. The comparison between the numerical results and the semi-analytic solution obtained at 300 meters from the source, on the surface, with  $\Delta x = \Delta y = 5 \text{ m}$  (10 points per wave length), is shown on figure 3.

We compute the same result with different spatial discretizations, with  $\Delta x = \Delta y$ . As expected, refining the spatial discretization decreases the error. With only 5 elements per wave length ( $\Delta x = \Delta y = 10 \text{ m}$ ), we get a poor accuracy due to the dispersion of the scheme : we observe oscillations after the simulated wave, due to the numerical dispersion of the scheme (see subsection 3.3). From 10 elements per wave length, however, we recover the semi-analytic solution with a pretty good accuracy. The accuracy of the method



(a) Horizontal displacement



(b) Vertical displacement

Figure 3: Displacement at the surface, 300 meters from source, with  $\Delta x = 5$  m,  $\Delta y = 5$  m (10 points per wave length)

cannot therefore compare with that of spectral elements (5 points per wave length), but it gives better results than classic second-order finite elements (30 points per wave length), and mostly on the surface, where we recover the non-dissipative Rayleigh wave. This is probably due to the introduction of parameter  $\theta$  which helps us simulate the rotation of the particle precisely, instead of recovering it with a Taylor development of the displacement, thus losing one order of accuracy for rotation. If we measure the  $L^\infty$ -error on vertical displacement at 300 meters from the source, with an angle of  $60^\circ$  with the horizontal axis, and plot its logarithm against the logarithm of the spatial step, we can see that we approximately have a slope of 2 fitting the points (figure 4). This confirms the results of subsection 3.1 as to the second-order nature of the

spatial scheme.

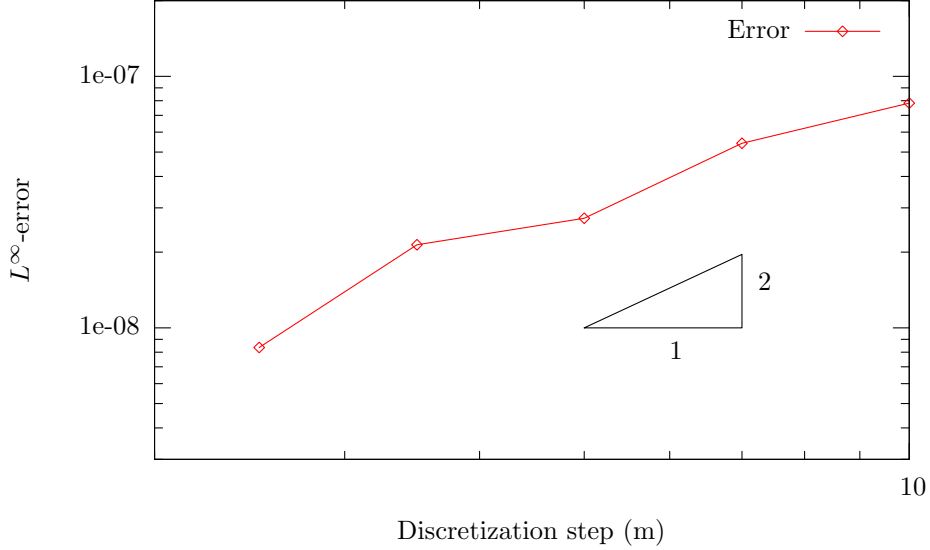


Figure 4: Linear fitting of the log-log diagram for the numerical error against the spatial discretization step

#### 4. Hamiltonian structure of the system of particles in continuous time

The elastodynamic equations are energy and momentum preserving when no exterior force is applied on the system. This important property should therefore be approximated by the scheme in order to reproduce correctly the behavior of the material. If we can exhibit an Hamiltonian structure in the dynamics of the system of particles, a perfect time-integration of the system will yield an exact conservation of energy and momentum in the isolated system. We shall address the problem of conservation of the Hamiltonian structure by the time-scheme in section 5. Numerically, this property is also crucial : if we are able to preserve an energy, or at least bound its error, we can ensure the stability of the system over long time simulations.

We denote by  $\dot{\square}$  time derivation  $\frac{d}{dt}\square$ . We denote by the subscript  $(IJ)$  the summation over all links between two particles ; we therefore have :

$$\sum_{(IJ)} \square = \frac{1}{2} \sum_I \sum_J \square$$

We shall be using more general notations in this section and in the next section to underline the similarity between displacement and rotation, and to use classical Hamiltonian notations. We set :

- We gather in  $\underline{Q}_T = (\underline{X}_1, \dots, \underline{X}_N)^T$  all the vectors  $\underline{X}_I$ , where  $N$  is the number of particles.
- We gather in the block diagonal matrix  $\underline{Q}$  the matrices  $\underline{Q}_I$ .
- Similarly,  $\underline{M}$  gathers the  $m_I \underline{Id}_3$ ,  $\underline{R}$  gathers the  $\underline{R}_I$ ,  $\underline{R}^0$  gathers the  $\underline{R}_I^0$ , and  $\underline{D}$  gathers the  $\underline{D}_I$ .
- $\underline{P}_T = \underline{M} \cdot \underline{Q}_T$  is the linear momentum.
- We gather in  $\underline{\Omega}$  the  $\underline{\Omega}_I$ .
- $\underline{P}_R = \underline{j}(\underline{\Omega}) \cdot \underline{Q} \cdot \underline{D}$  is the angular momentum.

The Hamiltonian is then of the form :

$$H(\underline{Q}_T, \underline{Q}_{\underline{R}}, \underline{P}_T, \underline{P}_{\underline{R}}) = \frac{1}{2} \underline{P}_T^T \cdot \underline{M}^{-1} \cdot \underline{P}_T + \frac{1}{2} \text{tr} (\underline{P}_{\underline{R}} \cdot \underline{D}^{-1} \cdot \underline{P}_{\underline{R}}^T) + U(\underline{Q}_T, \underline{Q}_{\underline{R}})$$

where  $U(\underline{Q}_T, \underline{Q}_{\underline{R}})$  is the potential energy of the discrete system, which depends on the precise expression of forces and torques. In the linear elastic case, we express the potential energy as a sum of simpler energies :

$$U(\underline{Q}_T, \underline{Q}_{\underline{R}}) = U_t(\underline{Q}_T, \underline{Q}_{\underline{R}}) + U_d(\underline{Q}_T, \underline{Q}_{\underline{R}}) + U_f(\underline{Q}_{\underline{R}})$$

where :

- $U_t(\underline{Q}_T, \underline{Q}_{\underline{R}})$  accounts for the deformation of each link :

$$U_t(\underline{Q}_T, \underline{Q}_{\underline{R}}) = \frac{1}{2} \sum_{(IJ)} S_{IJ} \frac{E}{1+\nu} \frac{\Delta u_{IJ} \cdot \Delta u_{IJ}}{D_{IJ}^{eq}}$$

with :

$$\Delta u_{IJ} = \underline{Q}_{J,T} - \underline{Q}_{I,T} + \underline{Q}_{J,R} \cdot \underline{X}_J^0 P_{IJ} - \underline{Q}_{I,R} \cdot \underline{X}_I^0 P_{IJ}$$

- $U_d(\underline{Q}_T, \underline{Q}_{\underline{R}})$  accounts for the global deformation of each particle :

$$U_d(\underline{Q}_T, \underline{Q}_{\underline{R}}) = \frac{1}{2} \sum_I \frac{E\nu}{(1+\nu)(1-2\nu)} (V_I + 3 \frac{\nu}{1-2\nu} V_I^l) (\varepsilon_I^v)^2$$

with :

$$\varepsilon_I^v = \sum_{J \in \mathcal{V}_I} \frac{\alpha_{IJ}^l S_{IJ}}{V_I + 3 \frac{\nu}{1-2\nu} V_I} \Delta u_{IJ} \cdot \underline{n}_{IJ}$$

$$\underline{n}_{IJ} = \frac{\underline{Q}_{J,T} - \underline{Q}_{I,T}}{\|\underline{Q}_{J,T} - \underline{Q}_{I,T}\|}$$

- $U_f(\underline{Q}_{\underline{R}})$  accounts for the flexion of the links between particles :

$$U_f(\underline{Q}_{\underline{R}}) = - \sum_{(IJ)} S_{IJ} \frac{E}{D_{IJ}^{eq}} \left( \alpha_n (\underline{Q}_{J,R} \cdot \underline{n}_{IJ}^0) \cdot (\underline{Q}_{I,R} \cdot \underline{n}_{IJ}^0) + \alpha_s (\underline{Q}_{J,R} \cdot \underline{s}_{IJ}^0) \cdot (\underline{Q}_{I,R} \cdot \underline{s}_{IJ}^0) \right. \\ \left. + \alpha_t (\underline{Q}_{J,R} \cdot \underline{t}_{IJ}^0) \cdot (\underline{Q}_{I,R} \cdot \underline{t}_{IJ}^0) \right)$$

We want to write the equations of the evolution of the system in the form :

$$\dot{\underline{Q}}_T = \frac{\partial H}{\partial \underline{P}_T} \quad (27)$$

$$\dot{\underline{Q}}_{\underline{R}} = \frac{\partial H}{\partial \underline{P}_{\underline{R}}} \quad (28)$$

$$\dot{\underline{P}}_T = - \frac{\partial H}{\partial \underline{Q}_T} \quad (29)$$

$$\dot{\underline{P}}_{\underline{R}} = - \frac{\partial H}{\partial \underline{Q}_{\underline{R}}} + \underline{\Lambda} \cdot \underline{Q}_{\underline{R}} \quad (30)$$



where  $\underline{\underline{\Lambda}}$  is the symmetric matrix of the Lagrange multipliers associated with the constraint  $\underline{\underline{Q}}_R^T \cdot \underline{\underline{Q}}_R = \underline{\underline{Id}}$ .

Using the definitions, we easily find :

$$\dot{\underline{\underline{Q}}}_T = \underline{\underline{M}}^{-1} \underline{\underline{P}}_T = \frac{\partial H}{\partial \underline{\underline{P}}_T}$$

and :

$$\dot{\underline{\underline{Q}}}_{I,R} = \underline{\underline{j}}(\underline{\underline{\Omega}}_I) \cdot \underline{\underline{Q}}_{I,R} = \underline{\underline{P}}_{I,R} \cdot \underline{\underline{D}}_I^{-1} = \frac{\partial H}{\partial \underline{\underline{P}}_{I,R}}$$

For relations (29) and (30), we only need to derive the potential energies. We find :

$$\begin{aligned} \frac{\partial U_t}{\partial \underline{\underline{Q}}_{I,T}} &= - \sum_{J \in \mathcal{V}_I} \frac{S_{IJ}}{D_{IJ}^{eq}} \frac{E}{1+\nu} \underline{\underline{\Delta}} u_{IJ} \\ \frac{\partial U_d}{\partial \underline{\underline{Q}}_{I,T}} &= - \sum_{J \in \mathcal{V}_I} \frac{E\nu}{(1+\nu)(1-2\nu)} S_{IJ} \varepsilon_{IJ}^v \underline{\underline{n}}_{IJ}^\perp \end{aligned}$$

and using (14) :

$$\dot{\underline{\underline{P}}}_{I,T} = \sum_{J \in \mathcal{V}_I} \underline{\underline{F}}_{IJ}$$

the expression of forces (6) gives (29).

For rotations, we find :

$$\begin{aligned} \frac{\partial U_t}{\partial \underline{\underline{Q}}_{I,R}} &= - \sum_{J \in \mathcal{V}_I} \frac{S_{IJ}}{D_{IJ}^{eq}} \frac{E}{1+\nu} \underline{\underline{\Delta}} u_{IJ} \otimes \underline{\underline{X}}_I^0 P_{IJ} \\ \frac{\partial U_d}{\partial \underline{\underline{Q}}_{I,R}} &= - \sum_{J \in \mathcal{V}_I} \frac{E\nu}{(1+\nu)(1-2\nu)} S_{IJ} \varepsilon_{IJ}^v \underline{\underline{n}}_{IJ} \otimes \underline{\underline{X}}_I^0 P_{IJ} \\ \frac{\partial U_f}{\partial \underline{\underline{Q}}_{I,R}} &= - \sum_{J \in \mathcal{V}_I} S_{IJ} \frac{E}{D_{IJ}^{eq}} \left( \alpha_n (\underline{\underline{Q}}_{J,R} \cdot \underline{\underline{n}}_{IJ}^0) \otimes \underline{\underline{n}}_{IJ}^0 + \alpha_s (\underline{\underline{Q}}_{J,R} \cdot \underline{\underline{s}}_{IJ}^0) \otimes \underline{\underline{s}}_{IJ}^0 + \alpha_t (\underline{\underline{Q}}_{J,R} \cdot \underline{\underline{t}}_{IJ}^0) \otimes \underline{\underline{t}}_{IJ}^0 \right) \end{aligned}$$

On the other hand, using (15) and the definition of  $\underline{\underline{P}}_R$  in terms of  $\underline{\underline{\Omega}}_I$ , we find :

$$\begin{aligned} \underline{\underline{j}} \left( \sum_{J \in \mathcal{V}_I} \underline{\underline{M}}_{IJ} \right) &= \frac{d}{dt} \left( \underline{\underline{j}}(\underline{\underline{R}}_I \cdot \underline{\underline{\Omega}}_I) \right) \\ &= \dot{\underline{\underline{P}}}_{I,R} \cdot \underline{\underline{Q}}_{I,R}^T - \underline{\underline{Q}}_{I,R} \cdot \dot{\underline{\underline{P}}}_{I,R}^T \end{aligned}$$

As a consequence, a general solution for  $\dot{\underline{\underline{P}}}_R$  is of the form :

$$\dot{\underline{\underline{P}}}_{I,R} = \left( \frac{1}{2} \underline{\underline{j}} \left( \sum_{J \in \mathcal{V}_I} \underline{\underline{M}}_{IJ} \right) + \tilde{\underline{\underline{\Lambda}}}_I \right) \cdot \underline{\underline{Q}}_{I,R}$$

where  $\tilde{\underline{\underline{\Lambda}}}_I$  is a symmetric matrix.  $\frac{1}{2} \underline{\underline{j}} \left( \sum_{J \in \mathcal{V}_I} \underline{\underline{M}}_{IJ} \right)$  is therefore the skew-symmetric part of  $\dot{\underline{\underline{P}}}_{I,R}$ . As a consequence, using relation :

$$(\underline{\underline{a}} \otimes \underline{\underline{b}}) \cdot \underline{\underline{Q}} = \underline{\underline{a}} \otimes (\underline{\underline{Q}}^T \cdot \underline{\underline{b}})$$

for any  $\underline{\underline{a}}, \underline{\underline{b}}$  and  $\underline{\underline{Q}}$ , we write :

$$\frac{\partial U_t}{\partial \underline{\underline{Q}}_{I,R}} \cdot \underline{\underline{Q}}_{I,R}^T = - \sum_{J \in \mathcal{V}_I} \frac{S_{IJ}}{D_{IJ}^{eq}} \frac{E}{1+\nu} \underline{\underline{\Delta}} u_{IJ} \otimes (\underline{\underline{Q}}_{I,R} \cdot \underline{\underline{X}}_I^0 P_{IJ})$$

$$\begin{aligned} \frac{\partial U_d}{\partial \underline{Q}_{\underline{I},R}} \cdot \underline{Q}_{\underline{I},R}^T &= - \sum_{J \in \mathcal{V}_I} \frac{E\nu}{(1+\nu)(1-2\nu)} S_{IJ} \varepsilon_{IJ}^v n_{IJ} \otimes (\underline{Q}_{\underline{I},R} \cdot \underline{X}_I^0 P_{IJ}) \\ \frac{\partial U_f}{\partial \underline{Q}_{\underline{I},R}} \cdot \underline{Q}_{\underline{I},R}^T &= - \sum_{J \in \mathcal{V}_I} S_{IJ} \frac{E}{D_{IJ}^{eq}} \left( \alpha_n (\underline{Q}_{\underline{J},R} \cdot \underline{n}_{IJ}^0) \otimes (\underline{Q}_{\underline{I},R} \cdot \underline{n}_{IJ}^0) + \alpha_s (\underline{Q}_{\underline{J},R} \cdot \underline{s}_{IJ}^0) \otimes (\underline{Q}_{\underline{I},R} \cdot \underline{s}_{IJ}^0) \right. \\ &\quad \left. + \alpha_t (\underline{Q}_{\underline{J},R} \cdot \underline{t}_{IJ}^0) \otimes (\underline{Q}_{\underline{I},R} \cdot \underline{t}_{IJ}^0) \right) \end{aligned}$$

Denoting  $\text{symm}()$  and  $\text{skew}()$  the symmetric and skew-symmetric parts of a matrix, we note that for any  $\underline{a}$  and  $\underline{b}$  :

$$\underline{j}(\underline{a} \wedge \underline{b}) = -\text{skew}(\underline{a} \otimes \underline{b})$$

and using (8) and (10), we obtain :

$$\text{skew} \left( \frac{\partial H}{\partial \underline{Q}_{\underline{I},R}} \cdot \underline{Q}_{\underline{I},R}^T \right) = -\frac{1}{2} \underline{j} \left( \sum_{J \in \mathcal{V}_I} \underline{M}_{IJ} \right)$$

Setting :

$$\underline{\Lambda}_I = \text{symm} \left( \frac{\partial H}{\partial \underline{Q}_{\underline{I},R}} \cdot \underline{Q}_{\underline{I},R}^T \right) + \tilde{\Lambda}_I$$

we therefore get :

$$\dot{\underline{Q}}_{\underline{I},R} = -\frac{\partial H}{\partial \underline{Q}_{\underline{I},R}} + \underline{\Lambda}_I \cdot \underline{Q}_{\underline{I},R}$$

with  $\underline{\Lambda}_I$  a symmetric matrix, which concludes the fact that the dynamics of the system (14) and (15) is a constrained Hamiltonian system.

## 5. Preservation of the Hamiltonian structure after time discretization

### 5.1. Description of the scheme

We use the same notations as in section 4.

We have seen in section 4 that the model under study has a Hamiltonian structure. To recover this property after time discretization, we therefore use a symplectic time scheme. As the system (27)–(30) is a constrained Hamiltonian system [15, Sec VII.5], it is natural to use the following RATTLE scheme, developed by Andersen [1], with time-step  $\Delta t$  :

$$\underline{P}_{T,n+1/2} = \underline{P}_{T,n} - \frac{\Delta t}{2} \underline{\nabla}_T U(\underline{Q}_{T,n}, \underline{Q}_{R,n}) \quad (31)$$

$$\underline{P}_{R,n+1/2} = \underline{P}_{R,n} - \frac{\Delta t}{2} \underline{\nabla}_R U(\underline{Q}_{T,n}, \underline{Q}_{R,n}) + \frac{\Delta t}{2} \underline{\Lambda}_n \underline{Q}_{R,n} \quad (32)$$

$$\underline{Q}_{T,n+1} = \underline{Q}_{T,n} + \Delta t \underline{M}^{-1} \underline{P}_{T,n+1/2} \quad (33)$$

$$\underline{Q}_{R,n+1} = \underline{Q}_{R,n} + \Delta t \underline{P}_{R,n+1/2} \underline{D}^{-1} \quad (34)$$

$$\text{such that } \underline{Q}_{R,n+1}^T \cdot \underline{Q}_{R,n+1} = \underline{Id} \quad (35)$$

$$\underline{P}_{T,n+1} = \underline{P}_{T,n+1/2} - \frac{\Delta t}{2} \underline{\nabla}_T U(\underline{Q}_{T,n+1}, \underline{Q}_{R,n+1}) \quad (36)$$

$$\underline{P}_{R,n+1} = \underline{P}_{R,n+1/2} - \frac{\Delta t}{2} \underline{\nabla}_R U(\underline{Q}_{T,n+1}, \underline{Q}_{R,n+1}) + \frac{\Delta t}{2} \tilde{\Lambda}_{n+1} \underline{Q}_{R,n+1}, \quad (37)$$

$$\text{such that } \underline{Q}_{R,n+1}^T \cdot \underline{P}_{R,n+1} \cdot \underline{D}^{-1} + \underline{D}^{-1} \cdot \underline{P}_{R,n+1}^T \cdot \underline{Q}_{R,n+1} = \underline{0} \quad (38)$$

where  $\underline{\underline{\Lambda}}_n$  and  $\tilde{\underline{\underline{\Lambda}}}_n$  are symmetric matrices, the Lagrange multipliers associated with the constraints (35) and (38). In the above equations, we denoted :

$$\begin{aligned}\underline{\underline{\nabla}}_T U(\underline{Q}_{T,n}, \underline{Q}_{R,n}) &= \frac{\partial U}{\partial \underline{Q}_T}(\underline{Q}_{T,n}, \underline{Q}_{R,n}) \\ \underline{\underline{\nabla}}_R U(\underline{Q}_{T,n}, \underline{Q}_{R,n}) &= \frac{\partial U}{\partial \underline{Q}_R}(\underline{Q}_{T,n}, \underline{Q}_{R,n})\end{aligned}$$

We denote the scheme (31)–(38) by :

$$(\underline{Q}_{T,n+1}, \underline{Q}_{R,n+1}, \underline{P}_{T,n+1}, \underline{P}_{R,n+1}) = \Psi_{\Delta t}(\underline{Q}_{T,n}, \underline{Q}_{R,n}, \underline{P}_{T,n}, \underline{P}_{R,n})$$

The proof for RATTLE's symplecticity can be read in [30]. As a consequence, in the absence of exterior forces, the energy of the system is an invariant of the system, and is preserved by the numerical integration in time. More precisely, the error is of order  $\mathcal{O}(e^{-\frac{\kappa}{\Delta t}})$  over a time period of  $e^{\frac{\kappa}{\Delta t}}$ , with  $\kappa > 0$  independent from  $\Delta t$  [15]. This yields the stability of the simulation over long time periods if the time step is chosen sufficiently small. In addition, we directly derive from (31)–(38) that the linear and angular momentum are exactly preserved.

Another important property of the RATTLE scheme is its reversibility. Starting with the knowledge of positions and velocities at time  $(n+1)\Delta t$ , we recover the positions and velocities at time  $n\Delta t$  with the following scheme :

$$(\underline{Q}_{T,n}, \underline{Q}_{R,n}, \underline{P}_{T,n}, \underline{P}_{R,n}) = \Psi_{-\Delta t}(\underline{Q}_{T,n+1}, \underline{Q}_{R,n+1}, \underline{P}_{T,n+1}, \underline{P}_{R,n+1})$$

As a reversible scheme, RATTLE is of even order, and as it is consistent, it is a second-order scheme.

RATTLE has the advantage of enforcing explicitly matrix  $\underline{Q}_{R,n}$  to be a rotation matrix, and at the same time be explicit in time. However, the nonlinearity of the constraint on  $\underline{Q}_{R,n}$  asks for an iterative algorithm, which will be addressed in section 5.3.

## 5.2. Implementation with forces and torques

For effective implementation of the RATTLE scheme, a difficulty arises from the fact that we do not necessarily have a direct access to  $\nabla U(\underline{Q}_{T,n}, \underline{Q}_{R,n})$ , as we compute the expression of forces and torques instead of the functional  $U$ . In the particular case studied here, we could impose directly  $U$  in the computation of velocity and position, but in that case, we would not be able to treat non-conservative exterior forces and torques, and the extension of the method to more complex behavior laws for the material would become unfeasible. The code would therefore lose its flexibility. To that end, we have chosen to recover the  $\nabla U(\underline{Q}_{T,n}, \underline{Q}_{R,n})$  from the expression of forces and torques.

For forces, the relation is simple :

$$\underline{\underline{\nabla}}_T U(\underline{Q}_T, \underline{Q}_R) = - \left( \sum_{J \in \mathcal{V}_I} \underline{F}_{IJ} \right)_I$$

For torques, we have :

$$\underline{\underline{\nabla}}_R U(\underline{Q}_T, \underline{Q}_R) = \dot{\underline{P}}_R - \underline{Q}_R \underline{\underline{\Lambda}}$$

where  $\underline{\underline{\Lambda}}$  is the symmetric matrix of Lagrange multipliers associated with constraint  $\underline{Q}_R \cdot \underline{Q}_R^T = Id$ . On the other hand,

$$\begin{aligned}\dot{\underline{j}} \left( \left( \sum_{J \in \mathcal{V}_I} \underline{M}_{IJ} \right) \right)_I &= \dot{\underline{P}}_R \cdot \underline{Q}_R^T + \underline{P}_R \cdot \dot{\underline{Q}}_R^T - \dot{\underline{Q}}_R \cdot \underline{P}_R^T - \underline{Q}_R \cdot \dot{\underline{P}}_R^T \\ &= \underline{Q}_R \cdot \underline{\underline{\nabla}}_R U(\underline{Q}_T, \underline{Q}_R)^T - \underline{\underline{\nabla}}_R U(\underline{Q}_T, \underline{Q}_R) \cdot \underline{Q}_R^T\end{aligned}$$

as the  $\underline{\underline{\Lambda}}$  are symmetric. Therefore, there exists a symmetric matrix  $\underline{\underline{\Lambda}}^0$  such that :

$$\underline{\underline{\nabla}}_R U(\underline{\underline{Q}}_T, \underline{\underline{Q}}_R) = \left( -\frac{1}{2} j \left( \left( \sum_{J \in \mathcal{V}_I} \underline{\underline{M}}_{IJ} \right) \right)_I - \underline{\underline{\Lambda}}^0 \right) \cdot \underline{\underline{Q}}_R$$

We denote :

$$\begin{aligned} \underline{\underline{\mathcal{F}}}_n &= \left( \sum_{J \in \mathcal{V}_I} \underline{\underline{F}}_{IJ} \right)_I \\ \underline{\underline{\mathcal{M}}}_n &= \left( \sum_{J \in \mathcal{V}_I} \underline{\underline{M}}_{IJ} \right)_I \end{aligned}$$

where forces  $\underline{\underline{F}}_{IJ}$  and torques  $\underline{\underline{M}}_{IJ}$  have been computed with positions  $\underline{\underline{Q}}_{T,n}$  and  $\underline{\underline{Q}}_{R,n}$ .

We can rewrite equations (31) to (37) as follows :

$$\underline{\underline{P}}_{T,n+1/2} = \underline{\underline{P}}_{T,n} + \frac{\Delta t}{2} \underline{\underline{\mathcal{F}}}_n \quad (39)$$

$$\underline{\underline{P}}_{R,n+1/2} = \underline{\underline{P}}_{R,n} + \frac{\Delta t}{4} j(\underline{\underline{\mathcal{M}}}_n) \underline{\underline{Q}}_{R,n} + \frac{\Delta t}{2} (\underline{\underline{\Lambda}}_n + \underline{\underline{\Lambda}}_n^0) \underline{\underline{Q}}_{R,n} \quad (40)$$

$$\underline{\underline{Q}}_{T,n+1} = \underline{\underline{Q}}_{T,n} + \Delta t \underline{\underline{M}}^{-1} \underline{\underline{P}}_{T,n+1/2} \quad (41)$$

$$\underline{\underline{Q}}_{R,n+1} = \underline{\underline{Q}}_{R,n} + \Delta t \underline{\underline{P}}_{R,n+1/2} \underline{\underline{D}}^{-1} \quad (42)$$

$$\text{such that } \underline{\underline{Q}}_{R,n+1}^T \cdot \underline{\underline{Q}}_{R,n+1} = \underline{\underline{Id}} \quad (43)$$

$$\underline{\underline{P}}_{T,n+1} = \underline{\underline{P}}_{T,n+1/2} + \frac{\Delta t}{2} \underline{\underline{\mathcal{F}}}_{n+1} \quad (44)$$

$$\underline{\underline{P}}_{R,n+1} = \underline{\underline{P}}_{R,n+1/2} + \frac{\Delta t}{4} j(\underline{\underline{\mathcal{M}}}_{n+1}) \underline{\underline{Q}}_{R,n+1} + \frac{\Delta t}{2} (\tilde{\underline{\underline{\Lambda}}}_{n+1} + \tilde{\underline{\underline{\Lambda}}}_{n+1}^0) \underline{\underline{Q}}_{R,n+1}, \quad (45)$$

$$\text{such that } \underline{\underline{Q}}_{R,n+1}^T \cdot \underline{\underline{P}}_{R,n+1} \cdot \underline{\underline{D}}^{-1} + \underline{\underline{D}}^{-1} \cdot \underline{\underline{P}}_{R,n+1}^T \cdot \underline{\underline{Q}}_{R,n+1} = \underline{\underline{0}} \quad (46)$$

We therefore see that we have the same type of problem as before to solve, the Lagrange multipliers  $\underline{\underline{\Lambda}}_n$  and  $\tilde{\underline{\underline{\Lambda}}}_n$  being replaced with the  $\underline{\underline{\Lambda}}_n + \underline{\underline{\Lambda}}_n^0$  and  $\tilde{\underline{\underline{\Lambda}}}_n + \tilde{\underline{\underline{\Lambda}}}_n^0$ .

In order to implement the scheme, without having to compute matrices  $\underline{\underline{\Lambda}}_n$  and  $\tilde{\underline{\underline{\Lambda}}}_n$ , we follow once more [15, Sec VII.5]. We set :

$$\begin{aligned} \underline{\underline{Y}}_n &= \underline{\underline{Q}}_{R,n}^T \cdot \underline{\underline{P}}_{R,n} \\ \underline{\underline{Z}}_{n+1/2} &= \underline{\underline{Q}}_{R,n}^T \cdot \underline{\underline{P}}_{R,n+1/2} \cdot \underline{\underline{D}}^{-1} \end{aligned}$$

We then have the following algorithm :

- We start the time step knowing  $\underline{\underline{Q}}_{T,n}$ ,  $\underline{\underline{Q}}_{R,n}$ ,  $\underline{\underline{Z}}_{n-1/2}$  and  $\underline{\underline{P}}_{T,n-1/2}$  (in the first step, these last two elements are the null matrix and the null vector).
- We compute the forces and torques in a submodule of the code, using only positions  $\underline{\underline{Q}}_{T,n}$  and  $\underline{\underline{Q}}_{R,n}$ .
- We then have the displacement scheme :

$$\begin{aligned} \underline{\underline{P}}_{T,n+1/2} &= \underline{\underline{P}}_{T,n-1/2} + \Delta t \underline{\underline{\mathcal{F}}}_n \\ \underline{\underline{Q}}_{T,n+1} &= \underline{\underline{Q}}_{T,n} + \Delta t \underline{\underline{M}}^{-1} \underline{\underline{P}}_{T,n+1/2} \end{aligned}$$

• Then, we use the rotation scheme :

– We compute  $\underline{Z}_{n+1/2}$  such that :

$$\begin{cases} \underline{Id} + \Delta t \underline{Z}_{n+1/2} \text{ is orthogonal} \\ \underline{Z}_{n+1/2} \cdot \underline{D} - \underline{D} \cdot \underline{Z}_{n+1/2}^T = \underline{D} \cdot \underline{Z}_{n-1/2} - \underline{Z}_{n-1/2}^T \cdot \underline{D} + \Delta t \underline{Q}_{\underline{R},n}^T \cdot \underline{j}(\underline{\mathcal{M}}_n) \cdot \underline{Q}_{\underline{R},n} \end{cases} \quad (47)$$

– We then compute :

$$\underline{Q}_{\underline{R},n+1} = \underline{Q}_{\underline{R},n} \cdot (\underline{Id} + \Delta t \underline{Z}_{n+1/2})$$

We can observe that all those steps are explicit, and that the only step that requires an iterative resolution is (47). Following [15], we use the quaternion iterative method to solve (47) for  $\underline{Z}_{n+1/2}$ . We describe that method in the next subsection.

### 5.3. Resolution of the nonlinear step

We set, for particle  $I$  :

$$\underline{A} = \underline{D}_I \cdot \underline{Z}_{I,n-1/2} - \underline{Z}_{I,n-1/2}^T \cdot \underline{D}_I + \Delta t \underline{Q}_{\underline{I},n}^T \cdot \underline{j}(\underline{\mathcal{M}}_{I,n}) \cdot \underline{Q}_{\underline{I},n}$$

Note that  $\underline{A}$  is a skew-symmetric matrix, which can be written as :

$$\underline{A} = \begin{pmatrix} 0 & -\alpha_3 & \alpha_2 \\ \alpha_3 & 0 & -\alpha_1 \\ -\alpha_2 & \alpha_1 & 0 \end{pmatrix}$$

Equation (47) now reads :

$$\begin{cases} \underline{Z}_{I,n+1/2} \cdot \underline{D}_I - \underline{D}_I \cdot \underline{Z}_{I,n+1/2}^T = \underline{A} \\ \left( \underline{Id} + \Delta t \underline{Z}_{I,n+1/2} \right) \cdot \left( \underline{Id} + \Delta t \underline{Z}_{I,n+1/2}^T \right) = \underline{Id} \end{cases} \quad (48)$$

To impose the second line of (48), we write the matrix  $\underline{Id} + \Delta t \underline{Z}_{I,n+1/2}$  with the quaternion notation :

$$\underline{Id} + \Delta t \underline{Z}_{I,n+1/2} = (e_0^2 + e_1^2 + e_2^2 + e_3^2) \underline{Id} + 2e_0 \underline{E} + 2\underline{E}^2$$

with :

$$\underline{E} = \begin{pmatrix} 0 & -e_3 & e_2 \\ e_3 & 0 & -e_1 \\ -e_2 & e_1 & 0 \end{pmatrix}$$

We have used the property that every orthogonal matrix can be written in this form, and that condition  $e_0^2 + e_1^2 + e_2^2 + e_3^2 = 1$  ensures that such a matrix is orthogonal. Equation (47) is hence equivalent to solving for  $e_0, e_1, e_2, e_3$  the following quadratic system of equations :

$$\begin{cases} 2(d_2 + d_3)e_0e_1 + 2(d_2 - d_3)e_2e_3 = \Delta t \alpha_1 \\ 2(d_1 + d_3)e_0e_2 + 2(d_3 - d_1)e_1e_3 = \Delta t \alpha_2 \\ 2(d_1 + d_2)e_0e_3 + 2(d_1 - d_2)e_1e_2 = \Delta t \alpha_3 \\ e_0^2 + e_1^2 + e_2^2 + e_3^2 = 1 \end{cases} \quad (49)$$

where :

$$d_i = \frac{I_1 + I_2 + I_3}{2} - I_i, \quad i = 1, 2, 3$$

Existence and uniqueness do not hold for this set of equations. In the simple case where  $\alpha_1 = \alpha_2 = \alpha_3 = 0$ , there are distinct solutions for  $(e_0, e_1, e_2, e_3) : (1, 0, 0, 0)$  (in that case,  $\underline{Z}_{n+1/2} = \underline{Id}$ ),  $(0, 1, 0, 0)$  (in that case,

$\underline{Z}_{n+\frac{1}{2}}$  represents the axial symmetry around axis  $x$ ),  $(0, 0, 1, 0)$  (associated with the axial symmetry around axis  $y$ ),  $(0, 0, 0, 1)$  (associated with the axial symmetry around axis  $z$ ), and their opposites which represent the same transformation. There is a deep physical reason for that non-uniqueness : dynamically speaking, the rigid body is totally represented by its equivalent inertia ellipsoid (the ellipsoid with the same axes of inertia and moments of inertia), which is invariant under the axial symmetries around the inertial axes  $x$ ,  $y$  and  $z$ . As the rotation  $\underline{Id} + \Delta t \underline{Z}_{I,n+1/2}$  is an increment of the global rotation of the particle, we select a solution “close” to identity, in a certain sense.

The existence and uniqueness in a neighbourhood of identity can be obtained from the equivalent formulation of RATTLE using the discrete Moser-Veselov scheme, with a fixed point theorem applied on equation (17) of reference [14]. We have found an explicit bound on the time-step  $\Delta t$  in Appendix A for the iterative scheme to converge, and ensure existence and uniqueness in a neighbourhood of identity. We use the following iterative scheme [15] :

- We start with  $(e_0^0, e_1^0, e_2^0, e_3^0) = (1, 0, 0, 0)$  (which represents identity).
- At each step, we compute :

$$e_1^{k+1} = \frac{\Delta t \alpha_1 - 2(d_2 - d_3)e_2^k e_3^k}{2(d_2 + d_3)e_0^k} \quad (50)$$

$$e_2^{k+1} = \frac{\Delta t \alpha_2 - 2(d_3 - d_1)e_1^k e_3^k}{2(d_1 + d_3)e_0^k} \quad (51)$$

$$e_3^{k+1} = \frac{\Delta t \alpha_3 - 2(d_1 - d_2)e_1^k e_2^k}{2(d_1 + d_2)e_0^k} \quad (52)$$

$$e_0^{k+1} = \sqrt{1 - (e_1^{k+1})^2 - (e_2^{k+1})^2 - (e_3^{k+1})^2} \quad (53)$$

Let us introduce :

$$\mathcal{B}\left(\frac{\sqrt{2}}{2}\right) = \left\{ (e_0, e_1, e_2, e_3) / e_0^2 + e_1^2 + e_2^2 + e_3^2 = 1, e_1^2 + e_2^2 + e_3^2 < \frac{1}{2} \right\}$$

When the time-step  $\Delta t$  satisfies the condition :

$$\Delta t \left( \frac{|\alpha_1|}{I_1} + \frac{|\alpha_2|}{I_2} + \frac{|\alpha_3|}{I_3} \right) \leq \frac{\sqrt{21} - 3}{6}$$

the algorithm (50)–(53) converges with a geometrical speed to the unique solution in  $\mathcal{B}\left(\frac{\sqrt{2}}{2}\right)$ .

#### 5.4. Some numerical results

We have chosen two examples to illustrate the preservation of energy in large displacement over long-time simulations. The first example is the case of the clamped beam : a 1m long beam is clamped at one end, and a torque is initially applied at the other end. The section of the beam is 5cm  $\times$  5mm. The torque is then suppressed and the beam freely oscillates. We have discretized the beam with 20 elements for the length ( $\Delta x = 5$ cm), and one element in perpendicular directions. The physical characteristics are that of steel :  $E$  is equal to 210,000 MPa,  $\nu$  has the value 0.25. We simulate the system over 5,000,000 time-steps, corresponding to 58 oscillations of the beam. On figure 5), we observe an excellent preservation of the energy. The configuration of the beam at the moment of release of the free end is shown on figure 6.

In order to simulate a fully three-dimensional case, we modelled the evolution of a pinched cylinder. The cylinder has a radius of 1m, a height of 2m and a width of 1cm. The physical characteristics are that of steel. The cylinder is discretized with 50 elements on the perimeter, 20 elements on the height and one element in width. Opposite forces are applied on two sides of the cylinder, pinching it. at the initial time, the forces are removed, and the cylinder is left free. We simulate the system over 500,000 time-steps, corresponding to

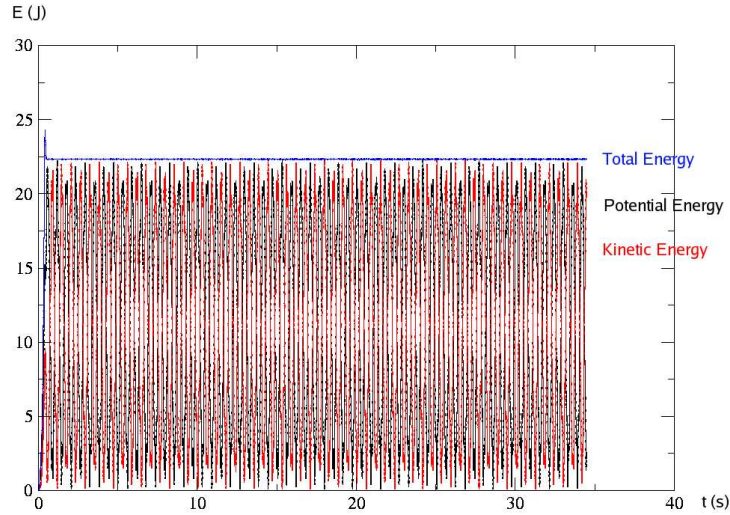


Figure 5: Total, potential and kinetic energies for the simulation of the clamped beam over 5000000 time-steps

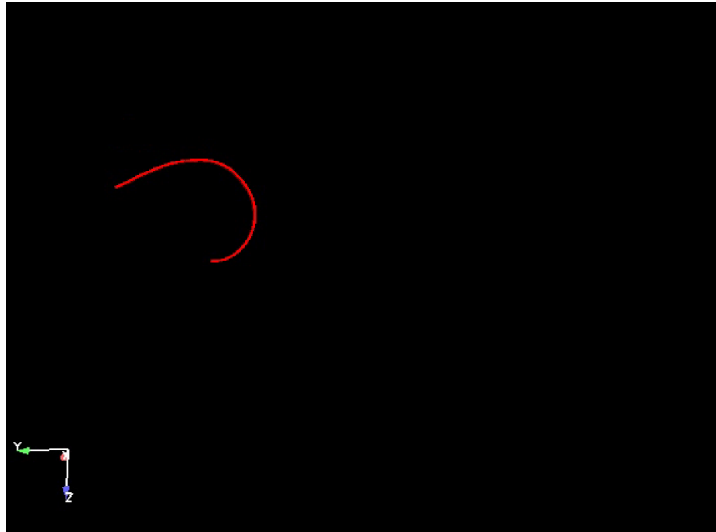


Figure 6: Initial configuration of the beam

45 oscillations of the cylinder. On figure 7, we again observe an excellent preservation of the energy. The configuration of the cylinder at the moment of release is shown on figure 8.

In both cases, the preservation of energy is quite good, even with large displacements in a three-dimensional geometry.

## 6. Conclusion

In this paper, we have shown that the scheme used by the CeaMka3D™ code is consistent with the equations of elastodynamics at order 2 in space and in time, and that we numerically recover the propagation of seismic waves in the body of the material and at the free surface, again with an accuracy  $\mathcal{O}(h^2)$  on the dispersion relation. Furthermore, we write the dynamics of the system in the form of a Hamiltonian dynamics. Using symplectic schemes, we correctly reproduce the preservation of the system energy. This

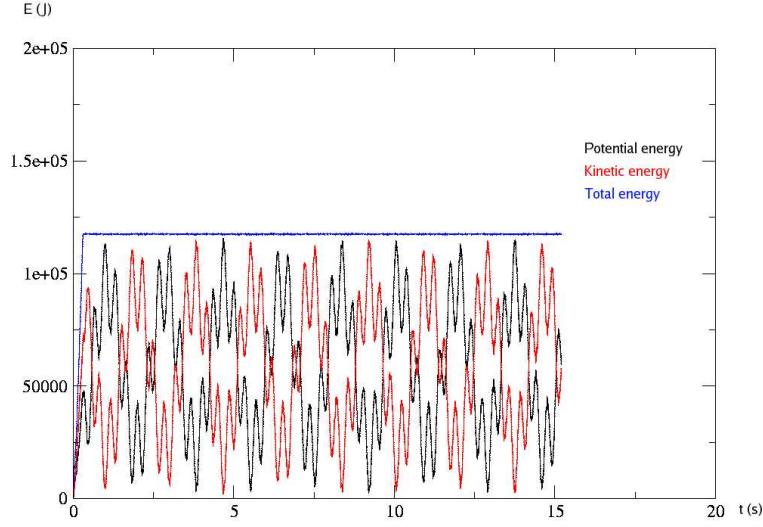


Figure 7: Total, potential and kinetic energies for the simulation of the cylinder over 500000 time-steps



Figure 8: Initial configuration of the cylinder

ensures numerical  $L^2$ -stability of the scheme, and allows long-time stable simulations with large displacements and large deformations. This work can be seen as a first step towards using more complex constitutive laws (while still maintaining stability of the scheme), and towards coupling the CeaMka3D™ code with a fluid code for fluid-structure interaction.

### Aknowledgements

The first author acknowledges the support of CEA under Grant n°1045.

We would like to thank Serge Piperno, Tony Lelièvre, Frédéric Legoll and Eric Cancès for useful discussions and advice on the mathematical and computational aspects of this paper. We also thank Karam Sab for pointing us the similarity of our model with Cosserat models. Thanks are also due to Gilles Vilmart for discussions of the resolution of the quaternion scheme.



## Appendix

### A. Resolution of the nonlinear step of the RATTLE time-scheme

In this appendix, we examine the resolution of the nonlinear step of the RATTLE time-scheme described in section 5.3. We determine conditions on the time-step  $\Delta t$  that ensure convergence of the iterative algorithm (50)–(53) in a certain neighbourhood of identity, and we conclude on the existence and uniqueness of a solution in this neighbourhood.

We denote  $\mathcal{B}(\underline{0}, r)$  the ball of center  $\underline{0}$  and radius  $r$  :

$$\mathcal{B}(\underline{0}, r) = \{(e_1, e_2, e_3) / e_1^2 + e_2^2 + e_3^2 < r^2\}$$

Using the numerical scheme described in section 5.3, we first show that it stabilizes a ball included in  $\mathcal{B}(\underline{0}, \frac{\sqrt{2}}{2})$ , under a CFL-type condition on  $\Delta t$ . We then show convergence in that same ball, and we conclude on convergence to the unique fixed point.

#### A.1. The iterative scheme is bounded

Starting with a given  $(e_0, e_1, e_2, e_3)$  computed in the previous iteration, such that  $e_0^2 + e_1^2 + e_2^2 + e_3^2 = 1$ , the iterative scheme (50)–(53) gives the new quadruplet  $(e_0^*, e_1^*, e_2^*, e_3^*)$  defined by :

$$\begin{aligned} e_1^* &= \frac{\Delta t \alpha_1 - 2(d_2 - d_3)e_2 e_3}{2(d_2 + d_3)e_0} \\ e_2^* &= \frac{\Delta t \alpha_2 - 2(d_3 - d_1)e_1 e_3}{2(d_1 + d_3)e_0} \\ e_3^* &= \frac{\Delta t \alpha_3 - 2(d_1 - d_2)e_1 e_2}{2(d_1 + d_2)e_0} \\ e_0^* &= \sqrt{1 - (e_1^*)^2 - (e_2^*)^2 - (e_3^*)^2} \end{aligned}$$

For this scheme to be well-defined,  $(e_1^*, e_2^*, e_3^*)$  should be in  $\mathcal{B}(\underline{0}, 1)$ . We impose a stronger condition, with  $(e_1, e_2, e_3)$  and  $(e_1^*, e_2^*, e_3^*)$  in  $\mathcal{B}(\underline{0}, \beta)$  where  $\beta$  is less than  $\frac{1}{2}$ .

Suppose that :

$$e_1^2 + e_2^2 + e_3^2 < \beta$$

We want to have :

$$(e_1^*)^2 + (e_2^*)^2 + (e_3^*)^2 < \beta$$

As  $e_0^2 + e_1^2 + e_2^2 + e_3^2 = 1$ , we also have  $e_0^2 > 1 - \beta$ . Since :

$$|e_2 e_3| \leq \frac{1}{2}(e_2^2 + e_3^2) < \frac{\beta}{2}$$

we obtain :

$$|e_1^*| < \frac{1}{2\sqrt{1-\beta}(d_2+d_3)} (|\Delta t \alpha_1| + \beta|d_2 - d_3|)$$

Let us define  $I_1 = d_2 + d_3$ ,  $I_2 = d_1 + d_3$ ,  $I_3 = d_1 + d_2$  and :

$$\begin{aligned} f(\beta) = \frac{1}{4(1-\beta)} \left[ \Delta t^2 \left( \frac{|\alpha_1|^2}{I_1^2} + \frac{|\alpha_2|^2}{I_2^2} + \frac{|\alpha_3|^2}{I_3^2} \right) + 2\beta \Delta t \left( \frac{|d_2 - d_3||\alpha_1|}{I_1^2} + \frac{|d_3 - d_1||\alpha_2|}{I_2^2} + \frac{|d_1 - d_2||\alpha_3|}{I_3^2} \right) \right. \\ \left. + \beta^2 \left( \frac{|d_2 - d_3|^2}{I_1^2} + \frac{|d_3 - d_1|^2}{I_2^2} + \frac{|d_1 - d_2|^2}{I_3^2} \right) \right] \end{aligned}$$

then the previous assumptions imply that :

$$(e_1^*)^2 + (e_2^*)^2 + (e_3^*)^2 < f(\beta)$$

Therefore, a sufficient condition for the scheme to be bounded is  $f(\beta) \leq \beta$ . We know that :

$$\frac{|d_2 - d_3|}{I_1} = \frac{|d_2 - d_3|}{d_2 + d_3} \leq 1$$

as the  $d_i$  are positive. Then :

$$f(\beta) \leq \frac{1}{4(1-\beta)} \left( \Delta t^2 \left[ \frac{|\alpha_1|^2}{I_1^2} + \frac{|\alpha_2|^2}{I_2^2} + \frac{|\alpha_3|^2}{I_3^2} \right] + 2\beta\Delta t \left( \frac{|\alpha_1|}{I_1} + \frac{|\alpha_2|}{I_2} + \frac{|\alpha_3|}{I_3} \right) + 3\beta^2 \right)$$

Hence, a sufficient condition for  $f(\beta) \leq \beta$  to hold is :

$$\Delta t^2 \left( \frac{|\alpha_1|^2}{I_1^2} + \frac{|\alpha_2|^2}{I_2^2} + \frac{|\alpha_3|^2}{I_3^2} \right) + 2\beta\Delta t \left( \frac{|\alpha_1|}{I_1} + \frac{|\alpha_2|}{I_2} + \frac{|\alpha_3|}{I_3} \right) + 7\beta^2 - 4\beta < 0 \quad (54)$$

Let us define :

$$B = \frac{|\alpha_1|}{I_1} + \frac{|\alpha_2|}{I_2} + \frac{|\alpha_3|}{I_3}$$

$$C = \frac{|\alpha_1|^2}{I_1^2} + \frac{|\alpha_2|^2}{I_2^2} + \frac{|\alpha_3|^2}{I_3^2}$$

A sufficient condition to obtain (54) is to have  $\Delta t \leq \tilde{\Delta}t$  with :

$$\tilde{\Delta}t = \frac{-2\beta B + \sqrt{4\beta^2 B^2 - 4(7\beta^2 - 4\beta)C}}{2C}$$

As we supposed that  $0 < \beta < \frac{1}{2} < \frac{4}{7}$ ,  $7\beta^2 - 4\beta < 0$ . We also know that  $B^2 \leq 3C$  and  $C \leq B^2$ , and it follows that :

$$\tilde{h} \geq \frac{2\sqrt{\frac{\beta - \beta^2}{3}} - \beta}{B}$$

In the end, we have the following lemma :

**Lemma A.1.** *Let us choose  $0 < \beta < \frac{1}{2}$  and  $\Delta t > 0$  such that :*

$$\Delta t \left( \frac{|\alpha_1|}{I_1} + \frac{|\alpha_2|}{I_2} + \frac{|\alpha_3|}{I_3} \right) \leq 2\sqrt{\frac{\beta - \beta^2}{3}} - \beta \quad (55)$$

If  $(e_1, e_2, e_3) \in \mathcal{B}(0, \sqrt{\beta})$ , then  $(e_1^*, e_2^*, e_3^*) \in \mathcal{B}(0, \sqrt{\beta})$ .

*A.2. The iterative scheme is a contraction*

Following the previous subsection, suppose that  $(e_1, e_2, e_3)$  and  $(f_1, f_2, f_3)$  are in  $\mathcal{B}(0, \sqrt{\beta})$ , and let  $e_0 = \sqrt{1 - e_1^2 - e_2^2 - e_3^2}$  and  $f_0 = \sqrt{1 - f_1^2 - f_2^2 - f_3^2}$ . We define  $e^*$  and  $f^*$  as before. We show here that  $\|e^* - f^*\| \leq \rho \|e - f\|$ , with  $0 < \rho < 1$ .

We compute :

$$e_1^* - f_1^* = \frac{(d_2 - d_3)}{I_1 e_0} \left[ (f_2 - e_2) \left( \frac{f_3 + e_3}{2} \right) + (f_3 - e_3) \left( \frac{f_2 + e_2}{2} \right) \right] + \frac{f_0 - e_0}{e_0} f_1^*$$

We then use the fact that  $\frac{|d_2-d_3|}{I_1} < 1$ . As the same type of results hold with a circular permutation of indices  $x, y$  and  $z$ , we let  $\|\cdot\|$  the euclidian norm in  $\mathbb{R}^3$  on  $(e_1, e_2, e_3)$ , and we find :

$$\begin{aligned} \|e^* - f^*\|^2 \leq & 2 \frac{\left(\frac{f_2+e_2}{2}\right)^2 + \left(\frac{f_3+e_3}{2}\right)^2}{e_0^2} (f_1 - e_1)^2 + 2 \frac{\left(\frac{f_1+e_1}{2}\right)^2 + \left(\frac{f_3+e_3}{2}\right)^2}{e_0^2} (f_2 - e_2)^2 \\ & + 2 \frac{\left(\frac{f_1+e_1}{2}\right)^2 + \left(\frac{f_2+e_2}{2}\right)^2}{e_0^2} (f_3 - e_3)^2 + \frac{4}{e_0^2} (f_2 - e_2)(f_3 - e_3) \left(\frac{f_2 + e_2}{2}\right) \left(\frac{f_3 + e_3}{2}\right) \\ & + \frac{4}{e_0^2} (f_1 - e_1)(f_3 - e_3) \left(\frac{f_1 + e_1}{2}\right) \left(\frac{f_3 + e_3}{2}\right) + \frac{4}{e_0^2} (f_1 - e_1)(f_2 - e_2) \left(\frac{f_1 + e_1}{2}\right) \left(\frac{f_2 + e_2}{2}\right) \\ & + 2 \frac{(f_1^*)^2 + (f_2^*)^2 + (f_3^*)^2}{e_0^2} (f_0 - e_0)^2 \end{aligned}$$

Since :

$$\frac{4}{e_0^2} (f_2 - e_2)(f_3 - e_3) \left(\frac{f_2 + e_2}{2}\right) \left(\frac{f_3 + e_3}{2}\right) \leq \frac{2}{e_0^2} \left[ (f_2 - e_2)^2 \left(\frac{f_2 + e_2}{2}\right)^2 + (f_3 - e_3)^2 \left(\frac{f_3 + e_3}{2}\right)^2 \right]$$

we have :

$$\|e^* - f^*\|^2 \leq \frac{2}{e_0^2} \left( \left\| \frac{e+f}{2} \right\|^2 \|e-f\|^2 + \|f^*\|^2 (f_0 - e_0)^2 \right)$$

We also have :

$$(f_0 - e_0)^2 \leq \frac{\left\| \frac{e+f}{2} \right\|^2}{\left(\frac{e_0+f_0}{2}\right)^2} \|e-f\|^2$$

In the end, we obtain the upper bound :

$$\|e^* - f^*\|^2 \leq 2 \frac{\left\| \frac{e+f}{2} \right\|^2}{e_0^2} \left( 1 + \frac{\|f^*\|^2}{\left(\frac{e_0+f_0}{2}\right)^2} \right) \|e-f\|^2$$

If we take the same hypotheses as in the first subsection, that is,  $(e_1, e_2, e_3) \in \mathcal{B}(\underline{0}, \sqrt{\beta})$  and  $(f_1, f_2, f_3) \in \mathcal{B}(\underline{0}, \sqrt{\beta})$ , and  $h$  such that  $(e_1^*, e_2^*, e_3^*) \in \mathcal{B}(\underline{0}, \sqrt{\beta})$  and  $(f_1^*, f_2^*, f_3^*) \in \mathcal{B}(\underline{0}, \sqrt{\beta})$ , then due to the convexity of  $\mathcal{B}(\underline{0}, \sqrt{\beta})$ , we have :

$$\left\| \frac{e+f}{2} \right\|^2 < \beta$$

and moreover, as  $e_0^2 > 1 - \beta$  et  $f_0^2 > 1 - \beta$ , then  $\left(\frac{e_0+f_0}{2}\right)^2 > 1 - \beta$ .

Then :

$$2 \frac{\left\| \frac{e+f}{2} \right\|^2}{e_0^2} \left( 1 + \frac{\|f^*\|^2}{\left(\frac{e_0+f_0}{2}\right)^2} \right) \leq 2 \frac{\beta}{1 - \beta} \left( 1 + \frac{\beta}{1 - \beta} \right) = \frac{2\beta}{(1 - \beta)^2}$$

In order to have a scheme which is a contraction, it is sufficient to impose :

$$\frac{2\beta}{(1 - \beta)^2} \leq 1$$

As  $0 < \beta < \frac{1}{2}$ , it is sufficient to choose :

$$\beta \leq 2 - \sqrt{3}$$

### A.3. Optimization on constant $\beta$

Optimizing the stability condition (55) on  $\Delta t$ , we obtain the following optimal value of  $\beta$  :

$$\beta_{\max} = \frac{7 - \sqrt{21}}{14} \approx 0.17$$

### A.4. Conclusion

If we take the time-step  $\Delta t$  such that :

$$\Delta t \left( \frac{|\alpha_1|}{I_1} + \frac{|\alpha_2|}{I_2} + \frac{|\alpha_3|}{I_3} \right) \leq 2\sqrt{\frac{\beta_{\max} - \beta_{\max}^2}{3}} - \beta_{\max} \approx 0.26$$

then the iterative scheme starting with  $(1, 0, 0, 0)$  converges to the unique solution of the nonlinear problem in  $\mathcal{B}(\underline{0}, \sqrt{\frac{7-\sqrt{21}}{14}})$ , and the convergence speed is geometric with a rate  $\rho < 1$ . In addition,  $\rho < 28 - 6\sqrt{21} \approx 0.5$ . We thus have proved existence and uniqueness of the solution in  $\mathcal{B}(\underline{0}, \frac{\sqrt{2}}{2})$ .

## References

- [1] H. C. Andersen. RATTLE: A "velocity" version of the SHAKE algorithm for molecular dynamics calculations. *J. Comput. Phys.*, 52(1):24–34, 1983.
- [2] C. Antoci, M. Gallati, and S. Sibilla. Numerical simulation of fluid-structure interaction by SPH. *Comput. Struct.*, 85(11–14, Sp. Iss. SI):879–890, 2007. 4th MIT Conference on Computational Fluid and Solid Mechanics, Cambridge, MA, JUN 13-15, 2007.
- [3] J. Bonet and T. S. L. Lok. Variational and momentum preservation aspects of Smooth Particle Hydrodynamic formulations. *Comput. Meth. Appl. Mech. Eng.*, 180(1–2):97–115, 1999.
- [4] P. A. Cundall and O. D. L. Strack. A discrete numerical model for granular assemblies. *Geotech.*, 29(1):47–65, 1979.
- [5] G. A. D’Addetta, F. Kun, and E. Ramm. On the application of a discrete model to the fracture process of cohesive granular materials. *Granul. Matter*, 4:77–90, 2002.
- [6] A. T. De Hoop. A modification of Cagniard’s method for solving seismic pulse problem. *Appl. Sci. Res.*, B8:349–356, 1960.
- [7] A. C. Eringen. Theory of micropolar elasticity. In H. Liebowitz, editor, *Fracture*, volume 2, pages 621–729. Academic Press, New York, 1968.
- [8] E. P. Fahrenthold and B. A. Horban. An improved hybrid particle-element method for hypervelocity impact simulation. *Int. J. Impact Engng.*, 26:169–178, 2001. Symposium on Hypervelocity Impact, Galveston, Texas, Nov 06-10, 2000.
- [9] E. P. Fahrenthold and R. Shivarama. Extension and validation of a hybrid particle-finite element method for hypervelocity impact simulation. *Int. J. Impact Engng.*, 29(1–10):237–246, 2003. Hypervelocity Impact Symposium, Noordwijk, Netherlands, Dec 07-11, 2003.
- [10] Y. T. Feng, K. Han, C. F. Li, and D. R. J. Owen. Discrete thermal element modelling of heat conduction in particle systems: Basic formulations. *J. Comp. Phys.*, 227(10):5072–5089, 2008.
- [11] S. Forest, F. Pradel, and K. Sab. Asymptotic analysis of heterogeneous Cosserat media. *Int. J. Solids Struct.*, 38:4585–4608, 2001.

- [12] R. A. Gingold and J. J. Monaghan. Smoothed Particle Hydrodynamics : Theory and application to nonspherical stars. *Mon. Not. R. Astron. Soc.*, 181:375–389, 1977.
- [13] O. Gonzalez. Exact energy and momentum conserving algorithms for general models in nonlinear elasticity. *Comput. Methods Appl. Mech. Eng.*, 190:1763–1783, 2000.
- [14] E. Hairer and G. Vilmart. Preprocessed discrete Moser-Veselov algorithm for the full dynamics of a rigid body. *J. Phys. A: Math. Gen.*, 39:13225–13235, 2006.
- [15] E. Hairer, C. Lubich, and G. Wanner. *Geometric Numerical Integration : Structure-Preserving Algorithms for Ordinary Differential Equations*, volume 31 of *Springer Series in Comput. Mathematics*. Springer-Verlag, 2nd edition, 2006.
- [16] K. Han, Y. T. Feng, and D. R. J. Owen. Coupled lattice Boltzmann and discrete element modelling of fluid-particle interaction problems. *Comput. Struct*, 85(11–14, Sp. Iss. SI):1080–1088, 2007. 4th MIT Conference on Computational Fluid and Solid Mechanics, Cambridge, MA, JUN 13-15, 2007.
- [17] P. Hauret and P. Le Tallec. Energy-controlling time integration methods for nonlinear elastodynamics and low-velocity impact. *Comput. Methods Appl. Mech. Eng.*, 195:4890–4916, 2006.
- [18] D. L. Hicks, J. W. Swegle, and S. W. Attaway. Conservative smoothing stabilizes discrete-numerical instabilities in SPH material dynamics computations. *Appl. Math. Comput.*, 85(2–3):209–226, 1997.
- [19] W. G. Hoover. *Smooth Particle Applied Mechanics : The State of the Art*, volume 25 of *Advanced Series in Nonlinear Dynamics*. World Scientific, 2006.
- [20] W. G. Hoover, W. T. Arhurst, and R. J. Olness. Two-dimensional studies of crystal stability and fluid viscosity. *J. Chem. Phys.*, 60:4043–4047, 1974.
- [21] A. Ibrahimbegovic and A. Delaplace. Microscale and mesoscale discrete models for dynamic fracture of structures built of brittle material. *Comput. Struct.*, 81(12):1255–1265, 2003.
- [22] J. C. Koo and E. P. Fahrenthold. Discrete Hamilton’s equations for arbitrary Lagrangian-Eulerian dynamics of viscous compressible flow. *Comput. Meth. Appl. Mech. Eng.*, 189(3):875–900, 2000.
- [23] S. Koshizuka and Y. Oka. Moving-particle semi-implicit method for fragmentation of incompressible fluid. *Nucl. Sci. Eng.*, 123:421–434, 1996.
- [24] S. Koshizuka, A. Nobe, and Y. Oka. Numerical analysis of breaking waves using the Moving Particle Semi-implicit method. *Int. J. Numer. Meth. Fluids*, 26:751–769, 1998.
- [25] S. Koshizuka, M. S. Song, and Y. Oka. A particle method for three-dimensional elastic analysis. In *Proc. 6th World Cong. Computational Mechanics (WCCM VI), Beijing*, September 5-10 2004.
- [26] F. Kun and H. Herrmann. A study of fragmentation processes using a discrete element method. *Comput. Meth. Appl. Mech. Engrg.*, 138(1–4):3–18, 1996.
- [27] H. Lamb. On the propagation of tremors over the surface of an elastic solid. *Phil. Trans. R. Soc. London; Ser. A*, 203:1–42, 1904.
- [28] T. A. Laursen and X. N. Meng. A new solution procedure for application of energy-conserving algorithms to general constitutive models in nonlinear elastodynamics. *Comput. Methods Appl. Mech. Engrg.*, 190: 6309–6322, 2001.
- [29] C. J. K. Lee, H. Noguchi, and S. Koshizuka. Fluid-shell structure interaction analysis by coupled particle and finite element method. *Comput. Struct.*, 85(11–14, Sp. Iss. SI):688–697, 2007. 4th MIT Conference on Computational Fluid and Solid Mechanics, Cambridge, MA, JUN 13-15, 2007.

- [30] B. J. Leimkuhler and R. D. Skeel. Symplectic numerical integrators in constrained hamiltonian systems. *J. Comput. Phys.*, 112(1):117–125, 1994.
- [31] L. D. Libersky, A. G. Petschek, T. C. Carney, J. R. Hipp, and F. A. Allahdadi. High strain Lagrangian hydrodynamics: A three-dimensional SPH code for dynamic material response. *J. Comput. Phys.*, 109(1):76–83, 1993.
- [32] L. B. Lucy. A numerical approach to the testing of the fission hypothesis. *Astron. J.*, 82:1013–1024, 1977.
- [33] C. Mariotti. Lamb’s problem with the lattice model Mka3D. *Geophys. J. Int.*, 171:857–864, 2007.
- [34] J. J. Monaghan. Simulating free surface flows with SPH. *J. Comput. Phys.*, 110(2):399–406, 1994.
- [35] D. O. Potyondy and P. A. Cundall. A bonded-particle model for rock. *Int. J. Rock Mech. Min. Sci.*, 41:1329–1364, 2004.
- [36] A. Ries, D. E. Wolf, and T. Unger. Shear zones in granular media: Three-dimensional contact dynamics simulation. *Phys. Rev. E*, 76(5, Part 1), 2007.
- [37] J. C. Simo, N. Tarnow, and K. K. Wong. Exact energy-momentum conserving algorithms and symplectic schemes for nonlinear dynamics. *Comput. Methods Appl. Mech. Eng.*, 100:63–116, 1992.
- [38] Y. Suzuki and S. Koshizuka. A Hamiltonian particle method for non-linear elastodynamics. *Int. J. Numer. Meth. Eng.*, 74(8):1344–1373, 2008.
- [39] J. W. Swegle, D. L. Hicks, and S. W. Attaway. Smoothed Particle Hydrodynamics stability analysis. *J. Comput. Phys.*, 116(1):123–134, 1995.
- [40] H. Yserentant. A new class of particle methods. *Numer. Math.*, 76(1):87–109, 1997.